Structure and dynamics of two-dimensional sheared granular flows

K. Anki Reddy and V. Kumaran
Department of Chemical Engineering, Indian Institute of Science, Bangalore 560 012, India
(Received 14 February 2009; published 10 June 2009)

The structure and dynamics of the two-dimensional linear shear flow of inelastic disks at high area fractions are analyzed. The event-driven simulation technique is used in the hard-particle limit, where the particles interact through instantaneous collisions. The structure (relative arrangement of particles) is analyzed using the bond-orientational order parameter. It is found that the shear flow reduces the order in the system, and the order parameter in a shear flow is lower than that in a collection of elastic hard disks at equilibrium. The distribution of relative velocities between colliding particles is analyzed. The relative velocity distribution undergoes a transition from a Gaussian distribution for nearly elastic particles, to an exponential distribution at low coefficients of restitution. However, the single-particle distribution function is close to a Gaussian in the dense limit, indicating that correlations between colliding particles have a strong influence on the relative velocity distribution. This results in a much lower dissipation rate than that predicted using the molecular chaos assumption, where the velocities of colliding particles are considered to be uncorrelated.

DOI: 10.1103/PhysRevE.79.061303 PACS number(s): 45.70.−n, 45.05.+x

I. INTRODUCTION

A dense granular material, which is a collection of discrete, solid particles dispersed in an interstitial fluid, is ubiquitous in nature, and in various industrial processes. A good understanding of the physics of granular materials is desired in order to design efficient processing and handling systems. The regime of dense flowing granular materials is an area of active research where a lot of progress has been made, but much further work remains to be done. Modeling of dense flows of two-dimensional disks in the hard-particle limit, where the interactions between particles can be modeled as instantaneous collisions, is the subject of the present study.

Flows of hard particles have been traditionally modeled using kinetic theory approaches, which draw an analogy between the motion of discrete particles in the granular material and the motion of molecules in a molecular gas. Kinetic theory calculations range from the more approximate approaches, where the Navier-Stokes equations are modified by adding a dissipation term due to inelastic collisions in the energy equation [1–4], to more sophisticated asymptotic approaches that used expansions in the inelasticity and the Knudsen number [5–8]. The important difference between a molecular gas and the granular flow of inelastic particles is that energy is not a conserved variable in a granular flow, since energy is dissipated in interparticle collisions. It has commonly been assumed that constitutive relations obtained using kinetic theory are limited in their applicability, mainly for two reasons. The first is that the binary collision approximation is inapplicable for dense flows of practical interest where multibody contacts are likely to dominate. However, there is recent evidence [9–11] to indicate that the binary contact approximation is, in fact, valid even for relatively dense flows. This is because extent of overlap between particles is determined by the volume fraction, and by the stiffness of contacts between particles. For perfect hard spheres where the stiffness tends to infinity, all contacts between particles are binary contacts even at high volume fraction, provided the material is flowing. As the stiffness decreases, the number of simultaneous contacts will increase. For materials of practical interest such as sand and glass, it is found that the stiffness of the contacts is sufficiently high that the particles are in the binary contact regime even when the volume fraction is as high as 0.56–0.58. The initial simulation studies [12] found multibody contacts because the stiffness of the contacts were assumed to be about 4 orders of magnitude lower than those for real particles in order to reduce computation time.

Even if the particle interactions are via binary contacts, kinetic theory calculations for dilute granular flows make the additional molecular chaos assumption, that the two-particle velocity distribution is the product of the single-particle distributions. In the case of dense granular flows, it is usual to use the Enskog approximation, that the two-particle distribution function is the product of the single-particle distributions and the equilibrium pair distribution function at contact. In the case of dense sheared elastic fluids, it is known that constitutive relations derived from kinetic theory are significantly in error, due to the effect of correlations [13]. Correlation effects are calculated using the ring-kinetic equation, where the three-particle distribution function is written as the product of two-particle distributions, and closure is effected at the two-particle level in the Bogoliubov-Born-Green-Kirkwood-Yvon (BBGKY) hierarchy. These correlations result in a viscosity that diverges as the logarithm of the strain rate in two dimensions, and the reason for this divergence is the slow decay (long-time tails) in the velocity autocorrelation function. In the case of sheared inelastic fluids, recent theoretical calculations [14,15] and experiments [16] indicate that long-time tails in the autocorrelation functions are not present. This is because the nature of the hydrodynamic modes in a sheared inelastic fluid, where energy is not a conserved variable, is very different from that in an elastic fluid. Therefore, kinetic theory calculations are valid for a larger range of volume fractions for sheared inelastic fluids, provided the coefficient of restitution is close to 1.

In the case of dense inelastic fluids, there are differences between the simulation results and the predictions of kinetic theory, especially for the rate of dissipation of energy in the

flow [9]. In addition, for the particular application of the flow down an inclined plane, the earlier constitutive relations [2] have consistently predicted that no stable flow is possible because the volume fraction increases as the angle of inclination increases, whereas stable flows have been observed in simulations. More sophisticated calculations which incorporate the Burnett contribution to the stress tensor have yielded realistic predictions for the variation in the volume fraction with the angle of inclination. However, there are significant numerical differences between the theoretical predictions and simulation results. This has led to suggestions [17–20] that long-range correlations are important, and kinetic theory cannot be applied for these flows. The presence of long-range correlations can be tested directly. Because simulations provide access to all the microscopic variables in the flow, it should be possible to calculate the correlation lengths directly in simulations. So far, soft-particle simulations have not yielded long-range correlations in the flow down an inclined plane. In the case of a sheared granular flow, contact dynamics simulations do report long-range contacts, but these have not been seen in event-driven simulations. The difference could be attributed to the difference in the simulation techniques, which are both hard-particle simulation techniques. The event-driven simulation technique proceeds from one discrete collision event to the next. In the contact dynamics simulations, interactions are considered to be due to hard-particle collisions, but the simulation proceeds in discrete time steps. All collisions that occur within one discrete time step are considered to be simultaneous contacts. Since the collision frequency diverges as the random-close-packing limit is approached, if the simulation time step is kept a constant, a larger fraction of collisions are considered to be simultaneous contacts. This explains the difference in the interpretation of simultaneous contacts in event-driven simulations and contact dynamics simulations.

A different approach for studying the structure and velocity correlations in three-dimensional dense shear flows was used [21,22], where event-driven simulations were used to extract the relative arrangement of particles as well as the distribution of relative velocities at contact. This analysis revealed several interesting and unusual features. The structure (relative arrangement of particles) in the flowing material is very different from that in a collection of elastic spheres at equilibrium. In the case of hard spheres at equilibrium, there is a crystallization from a random to an ordered phase at a volume fraction of 0.49. In contrast, in a sheared inelastic fluid, it was found that the system continues to be in a random state even at volume fractions as large as 0.5–0.6, provided the size of the simulation cell is large enough. Ordering does occur when the cell is small (less than about 5 particle diameters in width). The particle motion in the random state was found to be diffusive, in contrast to the particle motion by discrete cage-breaking events in the ordered state. The collision frequency for a sheared granular flow was found to be larger than that for particles at equilibrium, and it was found to diverge at a lower volume fraction than the random-close-packing volume fraction of 0.64 for a fluid of elastic spheres. The single-particle velocity distributions were found to be close to Gaussian distributions even at high volume fractions and low coefficients of restitution. However, the relative velocity of colliding particles along the line joining centers was very different from a Gaussian distribution, and it was well approximated by an exponential distribution at the lowest coefficient of restitution of 0.6. Mitarai and Nakanishi [23] also studied the effect of precollisional relative velocity in a dense granular flow, and noted a significant change in the form of the distribution, but did not proceed to model the exact form of the distribution. This change in the form of the distribution is due to the correlations in the velocities of particles, since the single-particle velocity distributions are Gaussian distributions. The correlation effects are not as strong in the direction perpendicular to the line joining centers, and the relative velocity distribution in this direction are found to be well fitted by Gaussian distributions. Empirical forms for the relative velocity distribution along the line joining centers were proposed. When these were used in the expressions for the collisional stress and dissipation rates, quantitative agreement with simulations was found. This indicates that the flow of dense granular materials can be quantitatively described by hard-particle models, which consider particle interactions to be instantaneous binary collisions, provided the effect of shear on the divergence of the collision frequency and the effect of correlations is incorporated in the relative velocity distribution.

Here, we study the shear flow of two-dimensional inelastic disks, with the objective of determining whether the unusual features observed in the flow of three-dimensional spheres are observed in two dimensions as well. The event-driven simulation technique is used, where the interactions between particles are considered to be instantaneous collisions. In three dimensions [21], the event-driven simulation technique suffers from the accumulation of numerical errors at very high volume or area fractions in both two and three dimensions, resulting in particle overlaps. In two dimensions, we also find the occurrence of shear banding for smooth particles when the coefficient of restitution is greater than about 0.9. Due to these errors, it is not possible to extend the simulation technique close to the random-close-packing limit, and we have been able to carry out simulations up to maximum area fractions of 0.81 for rough particles and 0.75 for smooth particles, depending on the coefficient of restitution.

II. COLLISION MODEL AND SIMULATION TECHNIQUE

The system consists of rough inelastic disks of diameter d subjected to uniform shear flow in the x-y plane. In the coordinate system used here, the flow is in the x direction, and the velocity gradient in the y direction. The particle mass m is set equal to 1 without loss of generality, so that all mass dimensions are nondimensionalized by the particle mass. The fluctuating velocity of the particles is defined as $\mathbf{c}=\mathbf{u}-\mathbf{U}$, while the fluctuating angular velocity is defined as $\varpi=\omega-\mathbf{\Omega}$, where $\mathbf{u}$ and ω are the particle velocity and angular velocity, and $\mathbf{U}$ and $\mathbf{O}$ are the mean velocity and angular velocity at the particle position. For a uniform shear flow, $\mathbf{U}$ is a linear function of the y coordinate, while Ω is independent of position. The collision rules used for calculating the change in the particle velocity and angular velocity are as

follows. Consider a collision between two particles with velocities $\mathbf{u}$ and $\mathbf{u}^*$, and angular velocities ω and ω^*, in which the unit vector in the direction of the line joining the centers of the particles from the particle at $\mathbf{x}$ to the particle at $\mathbf{x}^*$ is $\mathbf{k}$. In a collision that conserves linear and angular momenta, the sum of the velocities $(\mathbf{u}+\mathbf{u}^*)$ and the difference in the angular velocities $(\omega-\omega^*)$ are conserved in the collision.

The velocity difference between the two surfaces at contact, $\mathbf{g}$, can be written in indicial notation as $g_i=(u_i-u_i^*)-(\epsilon_{ijl}/2)k_j(\omega_l+\omega_l^*)$, where ϵ_{ijl} is the antisymmetric tensor, and $\mathbf{k}$ is the unit vector in the direction of the line joining the centers of the particles. The collision model used here is a rough-particle-collision model, in which the postcollisional relative velocities parallel and perpendicular to the line joining the centers of the particles are related by

$$g_i' k_i = -e_n g_i k_i, \tag{1}$$

$$\epsilon_{ijk} k_j g_k' = -e_t \epsilon_{ijk} k_j g_k, \tag{2}$$

where the normal coefficient of restitution e_n varies between 0 (perfectly inelastic collisions) and 1 (elastic collisions), and the tangential coefficient of restitution e_t varies between -1 (smooth particles) and $+1$ (perfectly rough particles). Energy is conserved in a collision for $e_n=1$ and $e_t=\pm 1$. From Eqs. (1) and (2), the particle velocity and angular velocity after collision are related to the velocity and angular velocity before collision by

$$u_i' - u_i = -[(1+e_n)/2](u_j-u_j^*)k_j k_i - [(1+e_t)/2][4I/(1+4I)] \times[(\delta_{ij}-k_i k_j)(u_j-u_j^*) - (\epsilon_{ijl}/2)k_j(\omega_l+\omega_l^*)], \tag{3}$$

$$\omega_i' - \omega_i = -[(1+e_t)/2][4I/(1+4I)](1/2I) \times[\epsilon_{ijl} k_j (u_l-u_l^*) + (1/2)(\delta_{ij}-k_i k_j)(\omega_j+\omega_j^*)], \tag{4}$$

where I is the moment of inertia scaled by the product of the mass and the square of the diameter of the particle.

The simulation procedure used here is an event-driven simulation procedure, where the trajectories of the particles are advanced forward in time, and the particles which collide in the shortest time are identified. All particles are advanced by this time period, and the collisional change in the velocities is implemented, before the next collision is predicted. We generate homogeneously sheared inelastic-hard-disk configurations using the Lees-Edwards boundary conditions [24], an event-driven nonequilibrium molecular-dynamics algorithm. The top and bottom boxes move with velocities $+U$ and $-U$, respectively, with respect to the central box. When a particle crosses the top (bottom) boundary of the central box with a horizontal velocity v_x, its image enters through the bottom (top) with a horizontal velocity $(v_x)_{image}=v_x \mp U$. This induces shear at the top (bottom) boundaries of the central box, which then propagates by collisions into the central box. All the simulations are carried out in square simulation cells with 1024 particles, and the area of the cell is adjusted to obtain the desired area fraction.

At high area fractions, the event-driven algorithm suffers from the disadvantage of inelastic collapse, where an infinite number of collisions take place between particles in a finite time. Inelastic collapse can be avoided by using a more realistic velocity-dependent coefficient of restitution which goes to 1 when the relative velocity goes to 0 [25] or by switching off inelasticity if the time between collisions is smaller than a minimum value [26]. The range of inelasticities for inelastic collapse in sheared granular flows is typically less than that for the homogeneous cooling state. Alam and Hrenya [27] carried out calculations for shear flow of smooth particles in two dimensions, and they reported that inelastic collapse happens at about $e_n=0.4$ for area fraction of about 0.5. When there is inelastic collapse, there are numerical errors due to the finite computational resolution of particle positions in the collision time prediction, which result in particle overlaps. In our simulations, we have taken care to ensure that there are no particle overlaps, and we have discarded simulation results where overlaps occur. Due to this, there is an upper limit on the area fractions, ϕ_{max}, listed in Table I, at which we have been able to obtain results. In contrast to the numerical limitations imposed by inelastic collapse, our simulation parameter range is also restricted by the physical limitation of shear localization, as shown in Figs. 1 and 2. As the area fraction is increased, the initially homogeneous sheared state evolves into a banded state, where the shear is localized in only one part of the domain. Flows with shear localization are also not considered in the present analysis. Shear localization provides a second physical upper bound on the area fractions accessible in the event-driven simulations. At coefficients of restitution greater than about 0.9, we find that the system transitions from a homogeneous shear flow to a shear localization regime before inelastic collapse. The area fraction for the transition from the homogeneous shear flow to a shear banded flow increases as the coefficient of restitution decreases. At coefficients of restitution below 0.9, there are numerical errors due to particle overlap first, and we do not observe shear localization for these coefficients of restitution. The maximum area fraction ϕ_{max} which can be simulated without particle overlaps decreases as the coefficient of restitution decreases.

TABLE I. Maximum area fraction ϕ_{max} at which there were no particle overlaps and no deviation from homogeneous shear at the end of a simulation run of 2104 collisions per particle for a 1024-particle system for both rough particles $(e_t=1)$ and smooth particles $(e_t=-1)$.

e_n	$\phi_{max}(e_t=-1.0)$	$\phi_{max}(e_t=1.0)$
0.98	0.74	0.75
0.95	0.76	0.77
0.90	0.79	0.81
0.80	0.81	0.81
0.70	0.77	0.80
0.60	0.73	0.79

III. STRUCTURE AND DYNAMICS

In two dimensions, the hexagonal order parameter for particles in contact is defined by

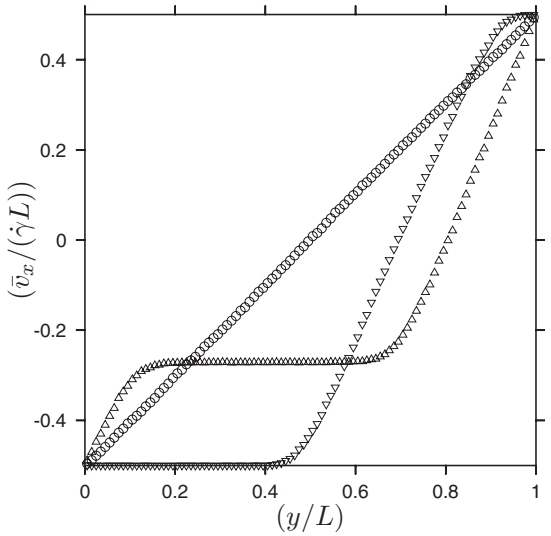

FIG. 1. Mean velocity, scaled by the product of the strain rate $\dot{\gamma}$ and box length L, as a function of y/L for the shear flow of smooth particles using Lees-Edwards boundary conditions, and for different area fractions and coefficients of restitution: ϕ=0.70 and e_n=0.98 (○), ϕ=0.76 and e_n=0.98 (△), and ϕ=0.79 and e_n=0.95 (▽).

$$q_m = \langle \exp(\imath m \theta_p) \rangle, \tag{5}$$

where $\langle\ \rangle$ is the average over all the bonds, and θ_p is the angle formed by a bond with respect to some arbitrary axis. The order parameter q_6 is 1 for a hexagonally ordered system, and is 0 for a completely random system. Since there are forces between particles only during collisions in the present system, we define the order parameter q_m as the sum over all binary collisions,

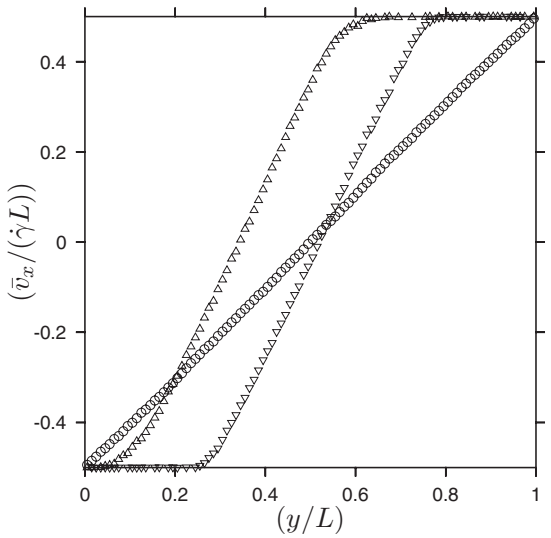

FIG. 2. Mean velocity, scaled by the product of the strain rate $\dot{\gamma}$ and box length L, as a function of y/L for the shear flow of rough particles using Lees-Edwards boundary conditions, and for different area fractions and coefficients of restitution: ϕ=0.75 and e_n=0.98 (○), ϕ=0.78 and e_n=0.98 (△), and ϕ=0.80 and e_n=0.95 (▽).

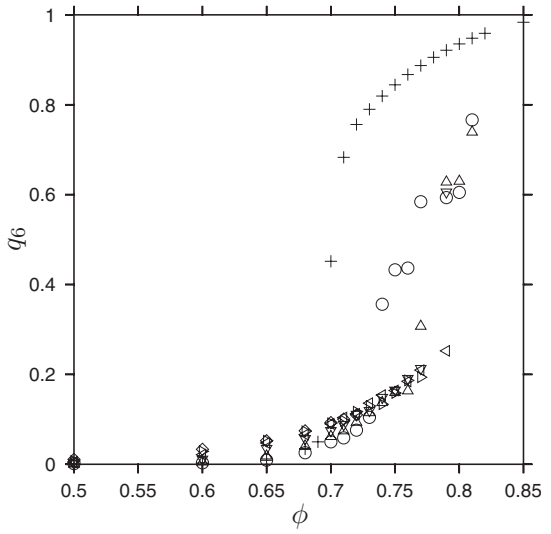

FIG. 3. Order parameter q_6 as a function of area fraction for smooth particles for different values of the normal coefficient of restitution: e_n=1.0 (+), e_n=0.98 (○), e_n=0.95 (△), e_n=0.9 (▽), e_n=0.8 (◁), e_n=0.7 (▷), and e_n=0.6 (◇).

$$q_m = (1/N_c) \sum_{\text{collisions}} \exp(\imath m \theta), \tag{6}$$

where N_c is the number of collisions, and the above average is carried out over all collisions. The q_6 values are shown as a function of packing fraction for a system size of 1024 particles at different coefficients of restitution in Fig. 3 for smooth particles and Fig. 4 for rough particles. For elastic disks, there is a crystallization transition at an area fraction of about 0.69 to a hexagonally ordered phase, signaled by a sharp increase in q_6 at this area fraction.

In a sheared system, we observe that the area fraction for the crystallization transition increases substantially. Even for

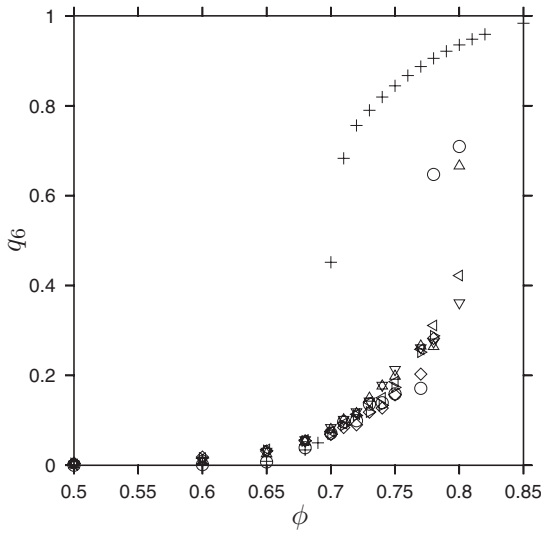

FIG. 4. Order parameter q_6 as a function of area fraction for rough particles with e_t=1.0 and for different values of the normal coefficient of restitution: e_n=1.0 (+), e_n=0.98 (○), e_n=0.95 (△), e_n=0.9 (▽), e_n=0.8 (◁), e_n=0.7 (▷), and e_n=0.6 (◇).

nearly elastic particles with e_n=0.98, the onset of ordering is at an area fraction of 0.73 for smooth particles, and at about 0.76 for rough particles. For lower coefficients of restitution of up to about 0.8, the increase in the order parameter takes place at an area fraction of between 0.78 and 0.8. When the coefficient of restitution is less than 0.7, we are unable to observe crystallization, because of the onset of numerical errors due to particle overlaps. It should be noted that the random-close-packing area fraction is 0.82 in two dimensions. Thus, our analysis indicates that shear increases the area fraction for the crystallization transition in two dimensions; this is similar to previously obtained results for three dimensions [21]. However, in three dimensions, it was found that there is virtually no ordering right up to the volume fractions at which the collision frequency diverged for coefficients of restitution less than about 0.8. This is not the case in two dimensions; we see signatures of ordering even at the lowest coefficient of restitution, e_n=0.6, considered here. This is consistent with previous results; it is well known that hexagonal ordering happens very efficiently in two dimensions, and the hexagonally ordered phase is topologically stable [28]. Specialized algorithms which impose rapid densification (analogous to quenching for thermal systems), such as the Woodcock (Monte Carlo) algorithm [29] and the Lubachevsky-Stillinger (molecular-dynamics) algorithm [30], are required to maintain the system in the random state. In three dimensions, though there is ordering, the face-centered-cubic phase is topologically unstable, and so it is easier to maintain the system in the random state [31].

The granular temperature is defined for rough disks as

$$3T = \langle (u_x - U)^2 \rangle + \langle u_y^2 \rangle + I\langle (\omega - \Omega)^2 \rangle, \tag{7}$$

where U and Ω are the mean linear and angular velocities, respectively. Note that the mass of the disks has been set equal to 1, without loss of generality, and I is the moment of inertia. For smooth disks, there is no rotational degree of freedom, and so the granular temperature is defined as

$$2T = \langle (u_x - U)^2 \rangle + \langle u_y^2 \rangle. \tag{8}$$

Since energy is not equally partitioned in a driven dissipative system, we also define the mean square of the velocities in the different directions as

$$T_x = \langle (u_x - U)^2 \rangle,$$

$$T_y = \langle u_y^2 \rangle,$$

$$T_\omega = I\langle (\omega - \Omega)^2 \rangle. \tag{9}$$

Instead of plotting the translational temperature itself, we show the ratio $T(1-e_n^2)/\dot{\gamma}^2 d^2$ in Fig. 5, because we expect the temperature to be proportional to $1/(1-e_n^2)$ at constant strain rate from energy balance conditions. Scaled in this manner, the temperature shows very little variation with the coefficient of restitution. Surprisingly, the temperature shows a slight increase as the area fraction is increased. We will see a little later that this is due to the reduction in the rate of dissipation of energy due to a change in the form of the relative velocity distribution at contact. However, it is important to note that the temperature neither decreases to zero nor

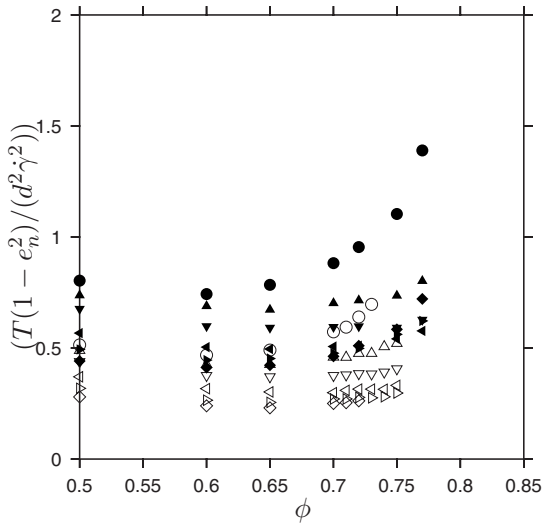

FIG. 5. The ratio $T(1-e_n^2)/d^2\dot{\gamma}^2$ as a function of area fraction for smooth particles (open symbols) and rough particles (filled symbols) and for e_n=0.98 (○), e_n=0.95 (△), e_n=0.9 (▽), e_n=0.8 (◁), e_n=0.7 (▷), and e_n=0.6 (◇).

diverges as the limit of close packing is approached for $e_n \leq 0.9$. This indicates that the efficiency of the collisional processes for shear production of energy and for inelastic dissipation of energy increases in proportion as the close-packing limit is approached, resulting in a finite temperature in this limit. It is also found that the temperature for rough inelastic particles is larger than that for smooth inelastic particles. The anisotropy in the temperature distribution, shown in Fig. 6, increases as the coefficient of restitution decreases, but it decreases as the area fraction decreases. The temperature in the flow direction is always found to be larger than that in the gradient direction and the temperature of the angular velocity fluctuations. For area fractions greater than about 0.7, the ratio of the temperatures in the different direc-

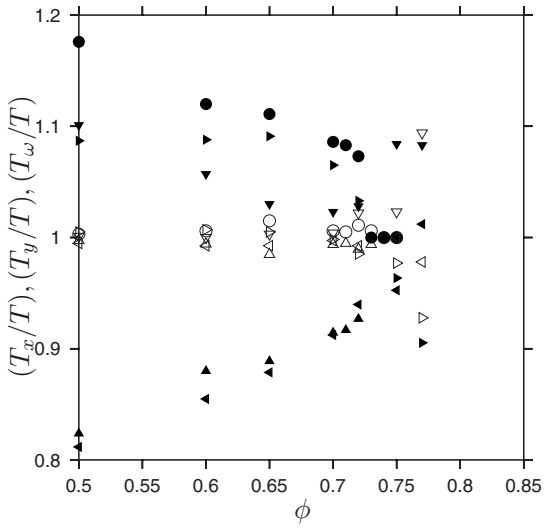

FIG. 6. The ratios T_x/T (○) and T_y/T (△) for smooth particles with e_t=−1, and the ratios T_x/T (▽), T_y/T (◁), and T_ω/T (▷) as functions of area fraction for coefficients of restitution e_n=0.98 (open symbols) and e_n=0.6 (filled symbols).

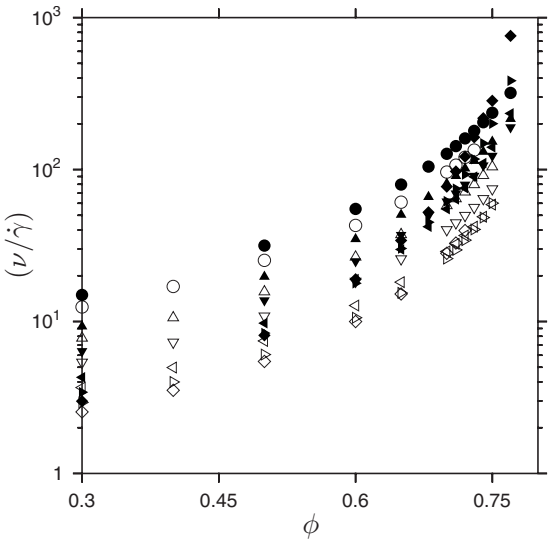

FIG. 7. The collision frequency ν scaled by the strain rate $\dot{\gamma}$ as a function of area fraction for smooth particles (open symbols) and rough particles (filled symbols) for different values of the normal coefficient of restitution: e_n=0.98 (○), e_n=0.95 (△), e_n=0.9 (▽), e_n=0.8 (◁), e_n=0.7 (▷), and e_n=0.6 (◇).

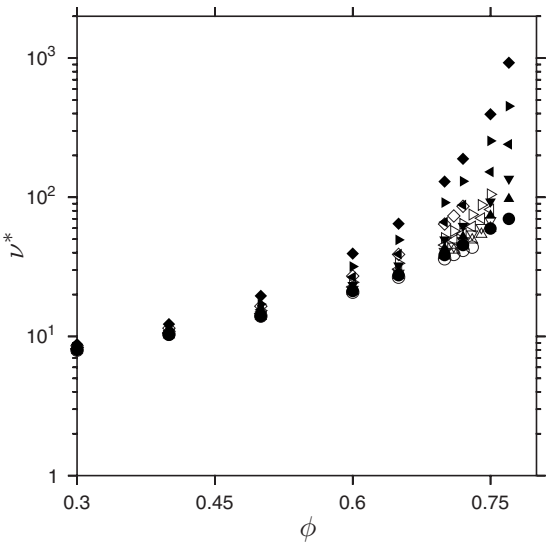

FIG. 8. The scaled collision frequency $\nu^*=\nu/\phi\sqrt{T}$ as a function of area fraction for smooth particles (open symbols) and rough particles (filled symbols) for different values of the normal coefficient of restitution: e_n=0.98 (○), e_n=0.95 (△), e_n=0.9 (▽), e_n=0.8 (◁), e_n=0.7 (▷), and e_n=0.6 (◇).

tions and the average temperature varies in a relatively small range between 0.9 and 1.1, indicating that equipartition is a good approximation for dense flows.

Next, we turn to the frequency of collisions for a dense flow ν, which is the number of collisions per particle per unit time. The collision frequency per unit area per unit time is $\rho\nu/2$, where ρ is the number of particles, and the factor (1/2) accounts for the double counting of collisions between two particles. The collision frequency scaled by the strain rate is shown in Fig. 7. It is clear that there is an increase of about 2 orders of magnitude when the area fraction increases from 0.3 to about 0.77, and this increase is much larger than that in the granular temperature. Since we have been able to carry out simulations for a higher area fraction for rough particles, we observe a higher collision frequency for rough particles. Another important feature observed in Fig. 7 is that the collision frequency appears to diverge at a lower area fraction as the coefficient of restitution decreases.

The kinetic theory framework can be used to place the collision frequency data in context. In the dilute limit, the collision frequency can be calculated using the kinetic theory of gases, and it is given by

$$\nu = (1 + e_n^{-1})\rho\sqrt{\pi T}, \tag{10}$$

where ρ is the number density (number per unit area, and T is the translational temperature [32]). However, as the area fraction increases, the collision frequency is greater than that predicted by kinetic theory, due to the excluded area and shadow effects. The collision frequency is then expressed as

$$\nu = (1 + e_n^{-1})\rho\chi(\phi)\sqrt{\pi T}, \tag{11}$$

where $\chi(\phi)$ is the pair distribution function, and Eq. (11) effectively defines the pair distribution function. For dense equilibrium hard disks, a widely used correlation for the pair distribution function for random configurations due to Torquato [33] is of the form,

$$\chi(\phi) = \frac{1 - 0.436\phi_f}{(1 - \phi_f)^2}\frac{\phi_c - \phi_f}{\phi_c - \phi} \tag{12}$$

for $\phi > \phi_f$, where ϕ_f=0.69 is the area fraction at the freezing transition, and ϕ_c=0.82 is the random-close-packing area fraction. Using this expression for the pair distribution the collision frequency is

$$\nu = \frac{4.268}{0.82 - \phi}. \tag{13}$$

It should be noted that the Torquato expression for the collision frequency is valid only for the random state, and not for the ordered state. Luding [34] derived a pair distribution function for a granular material in the absence of shearing which incorporated the effect of inelasticity,

$$\chi(\phi) = \chi_0(\phi) + \frac{\chi_f(\phi) - \chi_0(\phi)}{1 + \exp[-90.1(\phi - \phi_0)]}, \tag{14}$$

where $\chi_0=(1-7\phi)/(1-\phi)^2$ is the Carnahan-Starling expression for the pair distribution function, and $\chi_f = [(1+e_n)(\sqrt{\phi_c/\phi}-1)]^{-1}$, with ϕ_c=0.82 and ϕ_0=0.7006.

In order to make a comparison with the results for hard disks, a scaled collision frequency is defined as

$$\nu^* = \nu/\phi\sqrt{T}. \tag{15}$$

This scaled collision frequency is shown as a function of the area fraction in Fig. 8. In order to obtain an empirical form for the scaled collision frequency, we plot, in Fig. 9, the inverse of the scaled collision frequency $(1/\nu^*)$ as a function of area fraction for both rough and smooth particles.

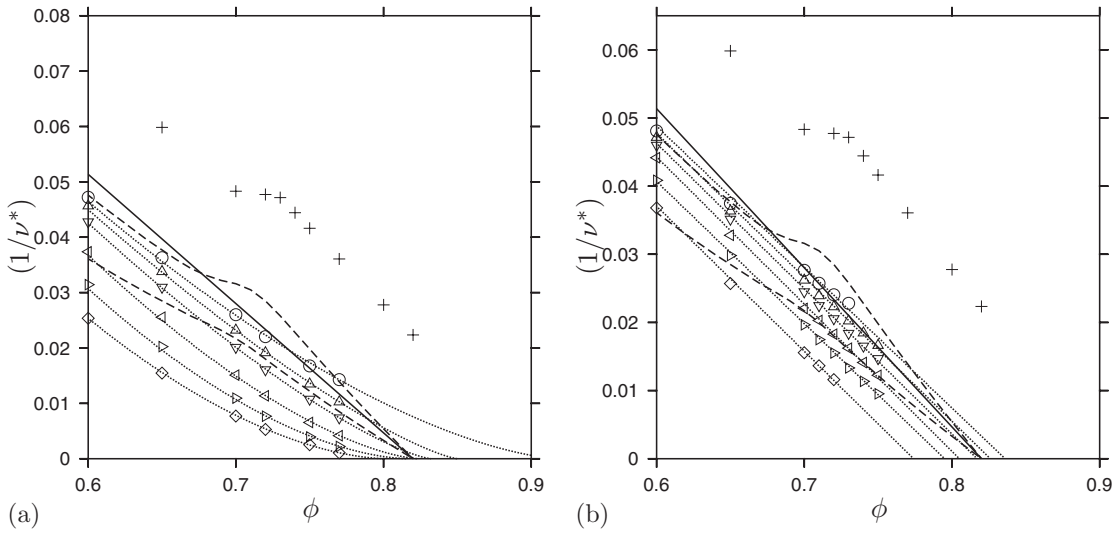

FIG. 9. The inverse of the scaled collision frequency $(1/\nu^*)$ as a function of area fraction for (a) rough particles and (b) smooth particles for different values of the normal coefficient of restitution: $e_n=1.0$ (+), $e_n=0.98$ (○), $e_n=0.95$ (△), $e_n=0.9$ (▽), $e_n=0.8$ (◁), $e_n=0.7$ (▷), and $e_n=0.6$ (◇). The solid line is the inverse of the collision frequency from the pair distribution function of Torquato equation (12), and the top and bottom dashed lines are the inverses of the collision frequency from the pair distribution functions of Luding equation (14) for $e_n=0.98$ and $e_n=0.6$, respectively.

Also shown in Fig. 9 is the inverse of the collision frequency for elastic particles. It should be noted that expression (13) is valid only for the random state. First, we note from Figs. 8 and 9 that the collision frequency for a sheared inelastic fluid is much higher than that for an elastic fluid at the same area fraction, and the collision frequency increases as the system becomes more inelastic (coefficient of restitution decreases). For an elastic fluid, the coefficient of restitution diverges at an area fraction of 0.91, which corresponds to the maximum hexagonal-close-packing area fraction for an ordered system. Also shown in Fig. 9 is expression (13) for the random configuration. As noted earlier, the random configurations have to be generated by specialized nonequilibrium algorithms where the particle diameter is increased in time. We have not attempted to carry out these simulations here, and instead we use the expression reported in previous studies [33,34]. The collision frequency for the random configurations diverges at the random-close-packing area fraction of 0.82 for both the pair distribution functions of Torquato equation (12) and the pair distribution function of Luding equation (14). For a sheared fluid with nearly elastic particles ($e_n=0.98$), we find that at area fractions less than about 0.75, the collision frequency is larger than that for that for the random state for an elastic fluid, and it follows the same trend as that given by Eqs. (13) and (14). However, as the area fraction increases beyond about 0.75, there is crystallization and the collision frequency approaches that for a crystallized elastic fluid. The divergence of the collision frequency takes place at an area fraction close to 0.91 for hexagonal close packing. When the coefficient of restitution is 0.8 or less, we do not see a clear transition to an ordered structure, and the collision frequency remains higher than that for the random state of a fluid of elastic particles. The pair distribution function of Luding [34] [Eq. (14)], which was derived for an unsheared granular material, captures the trend of increasing collision frequency with decreasing coefficient of restitution. However, this pair distribution function also diverges at the random-close-packing area fraction of 0.82, whereas the collision frequency in simulations appears to diverge at a lower area fraction for the sheared state. A similar phenomenon was also observed for a three-dimensional sheared granular material [21,22], where the volume fraction for the divergence of the frequency was termed the volume fraction ϕ_{ad} for arrested dynamics.

Analogously as with Eq. (13), we have attempted to obtain an empirical fit for the collision frequency,

$$\nu^* = \frac{A}{(\phi_{ad}-\phi)^a}, \tag{16}$$

where A, ϕ_{ad}, and a are functions of the coefficient of restitution. Here, ϕ_{ad} is the area fraction for arrested dynamics [21,22], since the collision frequency (and the stresses) diverges at fixed strain rate, or the strain rate goes to zero at fixed collision frequency. These coefficients were obtained using a least-squares fitting procedure using all the frequency data for $\phi \geq 0.5$. For every two adjacent data points $(\phi_i,(\nu_i^*)^{-1})$ and $(\phi_{i+1},(\nu_{i+1}^*)^{-1})$ in Fig. 9, we evaluate the error function

$$\text{error} = \{\log[(\nu_{i+1}^*)^{-1}] - \log[(\nu_i^*)^{-1}] - a[\log(\phi_{ad}-\phi_{i+1}) - \log(\phi_{ad}-\phi_i)]\}^2. \tag{17}$$

The average of the error function over all pairs of data points in Fig. 9 is then calculated as

$$\text{average error} = \frac{1}{N-1}\sum_{i=1}^{N-1}\{\log[(\nu_{i+1}^*)^{-1}] - \log[(\nu_i^*)^{-1}] - a[\log(\phi_{ad}-\phi_{i+1}) - \log(\phi_{ad}-\phi_i)]\}^2, \tag{18}$$

where N is the total number of data points in Fig. 9 in the

TABLE II. The coefficients ϕ_{ad}, a, and A in Eq. (16), and average error (18) for rough particles with $e_t=1.0$.

e_n	ϕ_{ad}	a	A	Error
0.98	0.920	1.56	3.64	0.318×10^{-3}
0.95	0.850	1.30	3.69	0.878×10^{-4}
0.90	0.832	1.33	3.39	0.397×10^{-4}
0.80	0.824	1.52	2.78	0.319×10^{-3}
0.70	0.817	1.71	2.39	0.596×10^{-3}
0.60	0.802	1.72	2.53	0.369×10^{-3}

TABLE III. The coefficients ϕ_{ad} and A in Eq. (16), and the average error from Eq. (18) for smooth particles with $e_t=-1.0$.

e_n	ϕ_{ad}	A	Error
0.98	0.836	4.84	0.490×10^{-3}
0.95	0.826	4.73	0.405×10^{-3}
0.90	0.817	4.69	0.298×10^{-3}
0.80	0.805	4.63	0.308×10^{-3}
0.70	0.795	4.79	0.469×10^{-3}
0.60	0.774	4.70	0.484×10^{-3}

area fraction greater than $\phi=0.5$ to $\phi=\phi_{max}$. The average error is then minimized with respect to the two constants ϕ_{ad} and a. After the constants ϕ_{ad} and a are evaluated, A is determined from Eq. (16).

The empirical constants obtained by the above fitting procedure are shown in Table II. It is observed that ϕ_{ad} is close to the hexagonal-close-packing area fraction for nearly elastic particles. However, for $e_n\leq0.8$, the value of ϕ_{ad} is lower than the random-close-packing area fraction $\phi_c=0.82$. The value of the coefficient a increases with a decrease in the coefficient of restitution, indicating that there is a sharper divergence in the frequency for inelastic particles than that for the random close packing of elastic particles. The only exception is for nearly elastic particles with $e_n=0.98$, which has a relatively high value of the coefficient a. This high value could be due to the transition from the random to the ordered state, which happens simultaneously with the divergence in the collision frequency. The collision frequency is similar to tracking that for the random state at low area fractions, and it crosses over to that for the ordered state as the area fraction increases. Due to this, the value of a appears to be higher than that for the random state.

For the case of smooth particles, we do not have sufficient data to obtain a fit of type (16). This is because shear banding occurs at an area fraction lower than the random-close-packing area fraction for nearly elastic particles, and we are not able to simulate a homogeneous system near the random-close-packing area fraction. Therefore, we have attempted to obtain an empirical fit using $a=1$ in Eq. (16). The coefficients A and ϕ_{ad} for this system are shown in Table III. As in the case of rough particles, we observe that the area fraction at which the collision frequency diverges is lower than that for random close packing. The only exception is for nearly elastic particles with $e_n=0.98$. The collision frequency is also significantly larger, for all area fractions that we were able to simulate, than the collision frequency for a system of elastic particles.

Figure 10 is a log-log plot of $1/\nu^*$ versus $\phi_{ad}-\phi$. From Fig. 10(a), the power-law dependence of $1/\nu^*$ on $\phi_{ad}-\phi$ is clearly visible, and it can be seen that the exponent a in Eq. (16) does vary as the coefficient of restitution is varied. In contrast, Fig. 10(b) shows that in the case of smooth particles, the exponent a is very close to 1, and even the prefactor A in Eq. (16) is remarkably independent of the coefficient of restitution. Thus, for smooth particles, the universal values of a and A in Eq. (16), which are independent of coefficient of restitution, can be used. In contrast, in the case of rough particles, it is necessary to incorporate the depen-

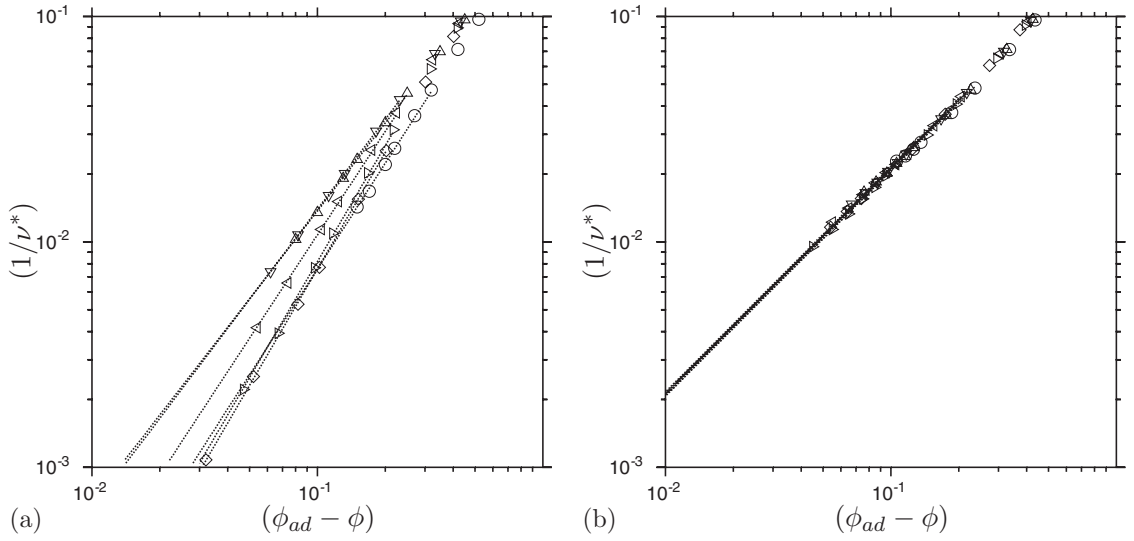

FIG. 10. Log-log plot of the inverse of the scaled collision frequency $1/\nu^*$ as a function of $\phi_{ad}-\phi$ for (a) rough particles and (b) smooth particles for different values of the normal coefficient of restitution: $e_n=1.0$ (+), $e_n=0.98$ (○), $e_n=0.95$ (△), $e_n=0.9$ (▽), $e_n=0.8$ (◁), $e_n=0.7$ (▷), and $e_n=0.6$ (◇). Here, ϕ_{ad} is given in Tables II and III.

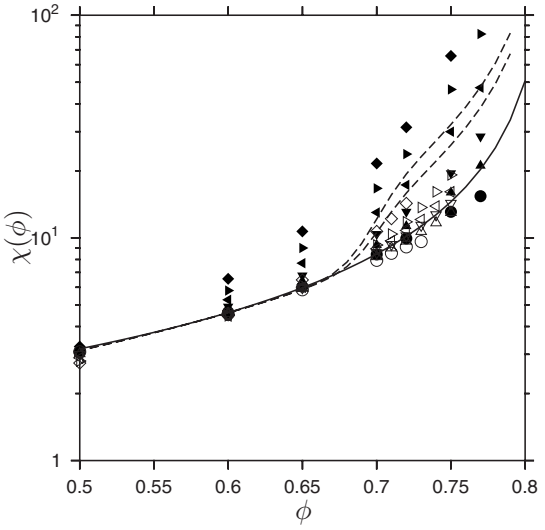

FIG. 11. The pair distribution function $\chi(\phi)$ as a function of area fraction for rough particles (filled symbols) and smooth particles (open symbols) for different values of the normal coefficient of restitution: e_n=0.98 (○), e_n=0.95 (△), e_n=0.9 (▽), e_n=0.8 (◁), e_n=0.7 (▷), and e_n=0.6 (◇). The solid line shows the pair distribution function of Torquato equation (12), while the top and bottom dashed lines show the pair distribution functions of Luding equation (14) for e_n=0.6 and e_n=0.98, respectively.

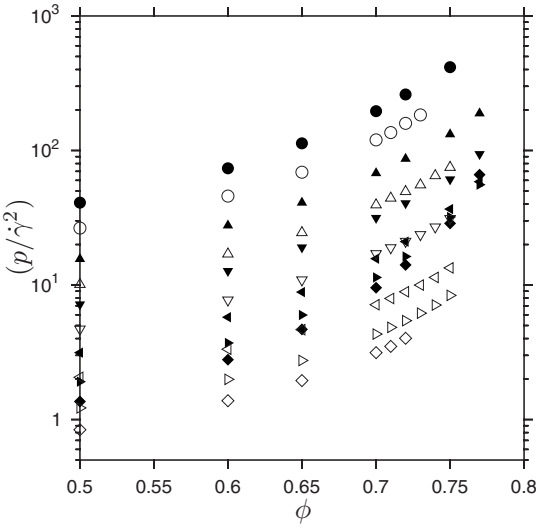

FIG. 12. The scaled pressure $(p/\dot{\gamma}^2)$ as a function of area fraction for rough particles (filled symbols) and smooth particles (open symbols) for different values of the normal coefficient of restitution: e_n=0.98 (○), e_n=0.95 (△), e_n=0.9 (▽), e_n=0.8 (◁), e_n=0.7 (▷), and e_n=0.6 (◇).

dence of a and A on the coefficient of restitution.

In order to make a comparison with kinetic theories for disks, it is necessary to calculate the pair distribution function using Eq. (11), and then insert this into the theoretical expressions for the pressure and the shear stress. The pair distribution function of Torquato [33] [Eq. (12)] is clearly lower than that observed in simulations (Fig. 11). The pair distribution function of Luding [34] [Eq. (14)], which was determined for an unsheared fluid, is clearly in closer agreement with simulation results. However, even this underestimates the pair correlation function for rough particles because it does not incorporate the fact that ϕ_{ad} for the sheared state is lower than the random-close-packing area fraction ϕ_c=0.82. For smooth particles, we do not have sufficient data near the close-packing area fraction to extract the exact divergence, due to the onset of shear banding. For the data obtained from simulations, it appears that fitting form (14) provides quite a good fit for the pair distribution function.

The underestimation of pair distribution function (11) is due to an underestimation of the collision frequency in the case of rough particles at high area fractions for coefficients of restitution less than about 0.8. Therefore, in the following analysis of the stress tensor and the dissipation rate, we use the actual pair distribution function obtained from the simulations for the comparison, and not the pair distribution function from previous theoretical studies.

The stress tensor in the simulations is the sum of a streaming and a collisional part. The streaming stress is given by

$$\sigma_{ij}^{s} = \langle \rho c_i c_j \rangle, \tag{19}$$

where ρ, the number density, is the number of particles per unit area (the mass of the particles is considered to be 1), and c_i and c_j are the fluctuating velocities. The collisional stress tensor is obtained using the expression

$$\sigma_{ij} = \frac{1}{A\tau} \sum_{\text{collisions}} (\Delta u_i) k_j, \tag{20}$$

where A is the simulation area, τ is the time over which averaging is carried out, $\Delta\mathbf{u}$ is the change in velocity of a particle during collision, and $\mathbf{k}$ is the unit vector in the direction of the line joining the centers of the particles. The total stress is determined as the sum of the streaming and collisional parts.

The total pressure, $p=(\sigma_{xx}+\sigma_{yy})/2$, is shown as a function of the area fraction at different coefficients of restitution in Fig. 12. The pressure is scaled in two ways in these figures. The scaled pressure $(p/\dot{\gamma}^2)$ is shown in Fig. 12, while the pressure scaled by the temperature (pd^2/T) is shown in Fig. 13. Note that the pressure has dimensions of force per unit length in two dimensions. It is observed that there is an increase of about 2 orders of magnitude in the pressure when scaled either by the square of the strain rate or the temperature. The pressure decreases as the coefficient of restitution decreases at constant strain rate, because the temperature decreases as the particles are made more inelastic. When scaled with the temperature, however, the pressure is remarkably independent of the coefficient of restitution for smooth particles, indicating that the equation of state is very insensitive to the coefficient of restitution for a sheared inelastic fluid. For rough particles, the pressure scaled by the temperature increases as the coefficient of restitution is decreased. The Jenkins-Richman [2] theory is close to the simulation results for nearly elastic particles, provided the pair distribution function from simulations is inserted into the theory. As the coefficient of restitution is decreased, the theory tends to overpredict the pressure.

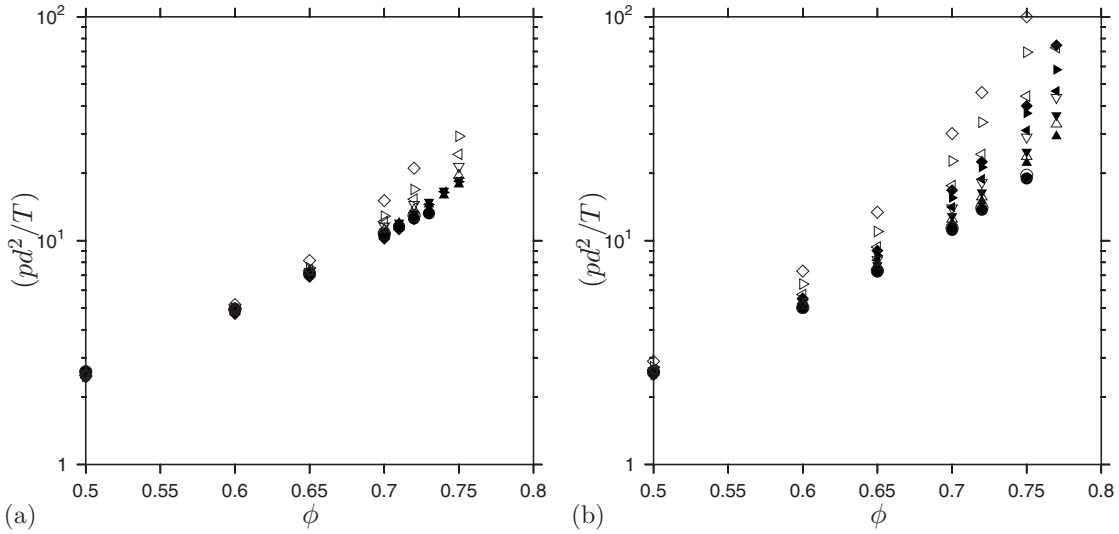

FIG. 13. The scaled pressure (pd^2/T) as a function of area fraction for (a) smooth particles and (b) rough particles for different values of the normal coefficient of restitution: e_n=0.98 (○), e_n=0.95 (△), e_n=0.9 (▽), e_n=0.8 (◁), e_n=0.7 (▷), and e_n=0.6 (◇). The filled symbols show the results from simulations, while the open symbols are the theoretical results of Jenkins and Richman [2] with the pair distribution function obtained from the event-driven simulations.

Another way to scale the pressure is using the collision frequency $pd/\nu\sqrt{T}$. This scaling is appropriate in the limit of high area fraction, where the transmission of stress is primarily collisional. Figure 14 shows the pressure scaled in this manner as a function of the area fraction. In contrast to the increase in pressure of 2 orders of magnitude in Fig. 12, we observe that the pressure scaled with the collisional frequency is remarkably invariant with area fractions even as the random-close-packing area fraction is approached. Even for the lowest coefficient of restitution e_n=0.9, the pressure decreases only by a factor of 2 when scaled by the collision frequency. This clearly indicates that the large increase in pressure in the close-packing limit is due to a similar increase in the collision frequency, while the average impulse in each collision (proportional to the fluctuating velocity of the particles) remains finite as the close-packing limit is approached.

The ratio of the shear stress to the pressure is shown in Fig. 15. It is clear from this figure that the ratio of the shear to normal stress approaches a constant value as the close-packing limit is approached. There are two significant results in this figure. The first is that the pressure and the shear stress diverge at the same area fraction, and not at two different area fractions. Further, since the ratio of the pressure and collision frequency is finite, the divergence of the shear stress also occurs at the same area fraction as the divergence of the frequency. From this, it can be inferred that as in the case of the pressure, the divergence in the shear stress is due to the divergence in the collision frequency as the close-packing area fraction is approached; the average impulse in a collision remains finite. A second significant result is that the divergence in the shear stress has the same power-law behavior as the divergence in the pressure, since the ratio is finite as the close-packing limit is approached.

The ratio of the shear stress to pressure also has another physical interpretation in the context of the flow down an inclined plane [12,35], since the ratio $\sigma_{xy}/p=\tan(\theta)$, where θ is the angle of inclination from the horizontal. For the presence of a stable flow, it is necessary for the $\tan(\theta)$ to increase as the area fraction is decreased from the close-packing limit. This implies that the slope of the σ_{xy}/p vs ϕ curve has to be negative in the close-packing limit. From Fig. 15, we observe that the slope of the σ_{xy}/p vs ϕ curve is positive for nearly elastic particles with coefficients of restitution greater than about 0.9, indicating that there will be no stable flow for nearly elastic particles. However, when the coefficient of restitution decreases below about 0.8, we observe that the ratio σ_{xy}/p increases as the area fraction is decreased near the

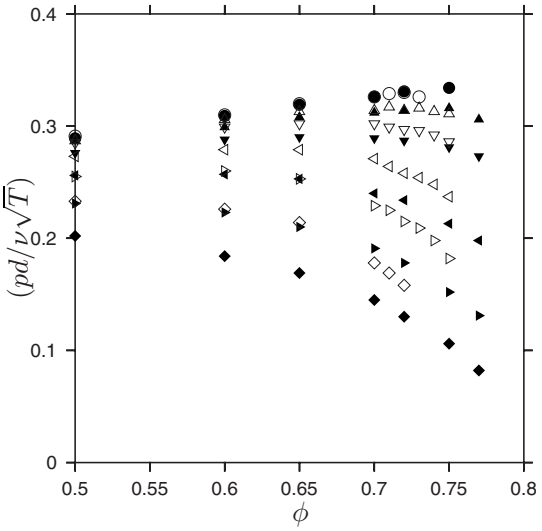

FIG. 14. The scaled pressure $(pd/\nu\sqrt{T})$ as a function of area fraction for rough particles (filled symbols) and smooth particles (open symbols) for different values of the normal coefficient of restitution: e_n=0.98 (○), e_n=0.95 (△), e_n=0.9 (▽), e_n=0.8 (◁), e_n=0.7 (▷), and e_n=0.6 (◇).

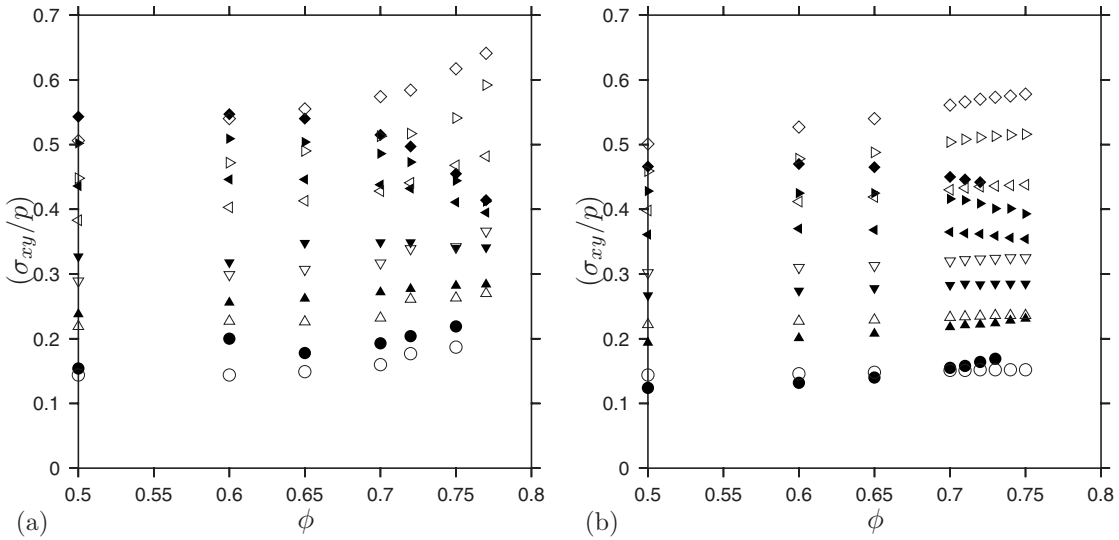

FIG. 15. The ratio of shear stress to pressure (σ_{xy}/p) as a function of area fraction for (a) rough particles and (b) smooth particles for different values of the normal coefficient of restitution: e_n=0.98 (○), e_n=0.95 (△), e_n=0.9 (▽), e_n=0.8 (◁), e_n=0.7 (▷), and e_n=0.6 (◇). The filled symbols show the simulation results, while the open symbols show the theory of Jenkins and Richman [2] with the pair distribution function determined from the simulations.

close-packing area fraction. This indicates that a stable flow is possible for relatively inelastic particles. Interestingly, we observe that the angle of inclination always increases with the area fraction if the constitutive relation is of the form proposed by Jenkins and Richman [2] for both smooth and rough particles. This is despite the fact that the numerical values of the ratio σ_{xy}/p obtained from the constitutive relations of Jenkins and Richman [2] are close to the simulation values obtained here.

The normal stress difference $[(\sigma_{xx}-\sigma_{yy})/p]$ is shown as a function of area fraction in Fig. 16. The normal stress difference has a maximum of about 0.2 for the lowest area fraction of 0.5 considered here, and it decreases as the area fraction increases. It is further observed that the normal stress difference is positive at low area fractions, but it becomes negative as the area fraction increases for highly inelastic particles. In the limit of close packing, the normal stress difference is numerically small for all coefficients of restitution, indicating that the approximation of an isotropic pressure is a good one in this case.

The rate of dissipation of energy per unit area is shown in Figs. 17 and 18 scaled in two ways. In Fig. 17, the rate of dissipation of energy is scaled by $T^{3/2}$. When scaled in this manner, the rate of dissipation of energy increases with area fraction in the close-packing limit. The increase is about 2 orders of magnitude when the area fraction increases from 0.5 to about 0.75. In the limit of high area fraction, it is more appropriate to scale the rate of dissipation of energy by the collision frequency, since the collision frequency diverges in this limit. The rate of dissipation of energy scaled in this manner, $D/\nu T(1-e_n^2)$, is shown as a function of area fraction in Fig. 18. It is clearly seen that when scaled in this manner, the rate of dissipation of energy decreases as the close-packing area fraction is approached, but the decrease is only by about a factor of 2 in the close-packing limit. This indicates that, as expected, it is more appropriate to scale the dissipation rate by the collision frequency in the limit of close packing.

There is a significant difference in the ratio $D/T^{3/2}$ between simulations and the theory of Jenkins and Richman [2], as shown in Fig. 17, even when the pair distribution function from the simulations is used in the theory. The theory predicts a much higher dissipation rate, and the difference is an order of magnitude for rough particles at e_n =0.6 and at the highest area fractions analyzed here. A similar difference was observed for a three-dimensional granular flow as well. The difference was because the distribution of relative velocities in theory is assumed to be a Gaussian dis-

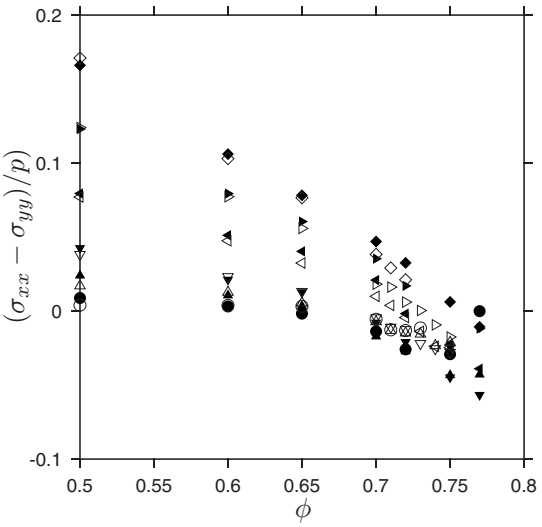

FIG. 16. The normal stress difference $[(\sigma_{xx}-\sigma_{yy})/p]$ as a function of area fraction for rough particles (filled symbols) and smooth particles (open symbols) for different values of the normal coefficient of restitution: e_n=0.98 (○), e_n=0.95 (△), e_n=0.9 (▽), e_n =0.8 (◁), e_n=0.7 (▷), and e_n=0.6 (◇).

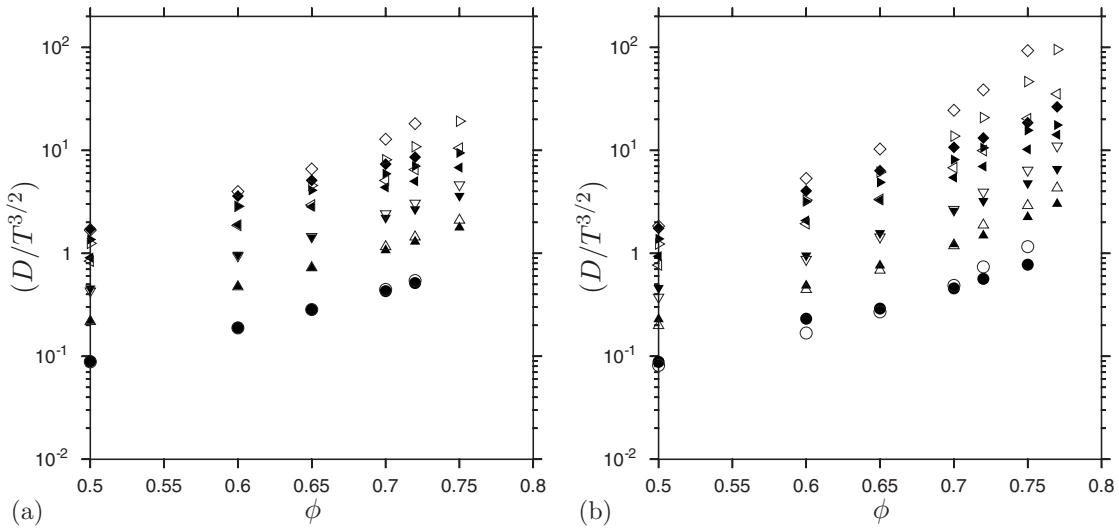

FIG. 17. The scaled rate of dissipation of energy $(D/T^{3/2})$ as a function of area fraction for (a) smooth particles and (b) rough particles for different values of the normal coefficient of restitution: e_n=0.98 (○), e_n=0.95 (△), e_n=0.9 (▽), e_n=0.8 (◁), e_n=0.7 (▷), and e_n=0.6 (◇). The filled symbols show the results from simulations, while the open symbols are the theoretical results of Jenkins and Richman [2] with the pair distribution function obtained from the simulations.

tribution. In simulations, it was found that the relative velocity distribution is very different from a Gaussian for $e_n \leq 0.8$, and the distribution function approaches an exponential distribution at the lowest coefficients of restitution analyzed. In Sec. IV, we analyze the relative velocity distribution in order to ascertain the cause of the difference in dissipation rates between theory and simulations.

IV. TWO-PARTICLE DISTRIBUTION FUNCTION

The transport of momentum and energy takes place primarily due to the collisional mechanism in the limit of high area fractions. These transport rates can be related to the distribution of the relative velocities for pairs of colliding particles. In a gas of elastic particles at equilibrium, the distribution of the relative velocities is a Gaussian distribution with a variance equal to two times the translational temperature. In a gas of inelastic particles under shear, it was found in [22] that the relative velocity distribution has an exponential form at low coefficients of restitution due to correlations between particles. Here, we examine whether correlations between particles alters the nature of the relative velocity distribution in the shear flow of inelastic disks.

In a steady shear flow, it is necessary to define the relative velocity distribution in terms of the difference in the absolute velocities of the colliding particles, rather than the difference in their fluctuating velocities. This is because the mean velocity $\mathbf{U}$ is a linear function of distance in the gradient direction. We consider two particles α and β with positions $\mathbf{x}_\alpha$ and $\mathbf{x}_\beta$, respectively, and consider the mean velocity to be zero at the location $\mathbf{x}_\alpha$. In this case, the relative velocity distribution is only a function of the separation between the two particles, $\mathbf{x}_{\alpha\beta}=(\mathbf{x}_\alpha-\mathbf{x}_\beta)$, and does not depend on the absolute positions of the two particles. The relative velocity distribution is defined as follows. The probability distribution that a particle α with position and velocity $(\mathbf{x}_\alpha,\mathbf{u}_\alpha,\omega_\alpha)$ is in contact with a second particle with position and velocity $(\mathbf{x}_\beta,\mathbf{u}_\beta,\omega_\beta)$, such that the unit vector from the center of particle α to β is $\mathbf{k}$, is defined as $F(\mathbf{x}_\alpha,\mathbf{u}_\alpha,\omega_\alpha,\mathbf{u}_\beta,\omega_\beta,\mathbf{k})$. Here, $\mathbf{u}_\alpha$, $\mathbf{u}_\beta$, ω_α, and ω_β are defined to be the precollisional velocities of the particles. For the purposes of calculating the stresses and dissipation rates, it is convenient to express the particle velocities in terms of the velocity of the center of mass, $\mathbf{v}$,

$$\mathbf{v} = (\mathbf{u}_\alpha + \mathbf{u}_\beta)/2, \tag{21}$$

and the velocity difference

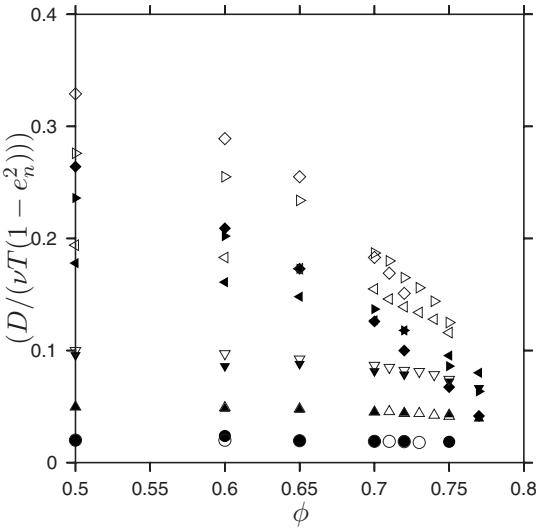

FIG. 18. The scaled rate of dissipation of energy $[D/\nu T(1-e_n^2)]$ as a function of area fraction for rough particles (filled symbols) and smooth particles (open symbols) for different values of the normal coefficient of restitution: e_n=0.98 (○), e_n=0.95 (△), e_n=0.9 (▽), e_n=0.8 (◁), e_n=0.7 (▷), and e_n=0.6 (◇).

$$\mathbf{w} = \mathbf{u}_\alpha - \mathbf{u}_\beta. \tag{22}$$

In a similar manner, the angular velocities of the two particles at contact can also be written in terms of the sum of the two angular velocities,

$$\upsilon = \omega_\alpha + \omega_\beta, \tag{23}$$

and one-half of the difference in angular velocities,

$$\varpi = (\omega_\alpha - \omega_\beta)/2. \tag{24}$$

It can easily be verified that the Jacobians for these two transformations is 1.

For the calculation of the stress and dissipation rates, it is sufficient to consider the distribution of relative velocities alone, since the collisional impulse depends only on the difference in velocities of the particles. The distribution of relative velocities is obtained by integrating the two-particle velocity distribution over the center-of-mass velocity and the sum of the angular velocities,

$$f(\mathbf{w},\upsilon,\mathbf{k}) = \int d\mathbf{v} \int d\varpi F(\mathbf{u}_\alpha,\mathbf{u}_\beta,\omega_\alpha,\omega_\beta,\mathbf{k}). \tag{25}$$

For future reference, we also define the reduced distributions $f_w(\mathbf{w},\mathbf{k})$ and $f_\upsilon(\upsilon,\mathbf{k})$ for the relative velocity and angular velocity, respectively,

$$f_w(\mathbf{w},\mathbf{k}) = \int d\upsilon f(\mathbf{w},\upsilon,\mathbf{k}), \tag{26}$$

$$f_\upsilon(\upsilon,\mathbf{k}) = \int d\mathbf{w} f(\mathbf{w},\upsilon,\mathbf{k}). \tag{27}$$

The relative velocity can also be resolved into its components along the line joining the centers of the particles (w_n), and perpendicular to the line joining the centers of the particles (w_t),

$$w_n = \mathbf{w}\cdot\mathbf{k}, \tag{28}$$

$$w_t = \mathbf{w}\cdot(\mathbf{k}\times\mathbf{e}_\perp), \tag{29}$$

where $\mathbf{e}_\perp$ is the unit vector in the direction perpendicular to the plane of flow. For two-dimensional disks, the direction of the angular velocity is always perpendicular to the plane of flow, so the angular velocity is a scalar. The reduced distributions for each of these velocity components can be written as

$$f_{wn}(w_n,\mathbf{k}) = \int d\upsilon \int dw_t f(\mathbf{w},\upsilon,\mathbf{k}), \tag{30}$$

$$f_{wt}(w_t,\mathbf{k}) = \int d\upsilon \int dw_n f(\mathbf{w},\upsilon,\mathbf{k}), \tag{31}$$

$$f_\upsilon(\upsilon,\mathbf{k}) = \int d\mathbf{w} f(\mathbf{w},\upsilon,\mathbf{k}). \tag{32}$$

The relative velocity distribution defined in Eq. (32) is a function of the orientation vector $\mathbf{k}$ of the line joining the centers of the disks at collision. It is convenient to describe this dependence using a Fourier expansion in the angle θ of the line joining centers with the flow direction,

$$f_{wn}(w_n,\mathbf{k}) = f_{wn}^{(0)}(\mathbf{w}) \sum_1^\infty [g_{wn}^{(n)}(\mathbf{w})\cos(n\theta) + h_{wn}^{(n)}(\mathbf{w})\sin(n\theta)], \tag{33}$$

where the component distributions $f_w^{(0)}$, $g_w^{(n)}$, and $h_w^{(n)}$ are given by

$$f_{wn}^{(0)} = \frac{1}{2\pi}\int_0^{2\pi} d\theta f_{wn}(\mathbf{w},\mathbf{k}), \tag{34}$$

$$g_{wn}^{(n)} = \frac{1}{\pi}\int_0^{2\pi} d\theta f_{wn}(\mathbf{w},\mathbf{k})\cos(n\theta), \tag{35}$$

$$h_{wn}^{(n)} = \frac{1}{\pi}\int_0^{2\pi} d\theta f_{wn}(\mathbf{w},\mathbf{k})\sin(n\theta). \tag{36}$$

Similar distributions can be defined for f_{wt} and f_υ, but these are not analyzed here, because the distributions of the tangential relative velocity and the relative angular velocity do not show large deviations from a Gaussian distribution. The largest deviation from a Gaussian distribution is for the relative normal velocity at contact, and so we analyze the functions $h_{wn}^{(n)}$ and $g_{wn}^{(n)}$ in further detail. Based on symmetry, $h_{wn}^{(1)}$ and $g_{wn}^{(1)}$ are zero. The distributions $g_{wn}^{(2)}$ and $h_{wn}^{(2)}$ are related to the normal stress difference and the shear stress, and so these are analyzed in further detail.

First, we analyze the isotropic component of the normal velocity distribution, $f_{wn}^{(0)}(w_n)$ in Eq. (33). Figures 19 and 20 show the relative velocity distribution for two different area fractions, ϕ=0.5 and ϕ=0.75, and for different coefficients of restitution. As noted earlier, for a dense gas of elastic particles in the absence of shear, the distribution of relative velocities is a Gaussian distribution with variance equal to two times the translational temperature. For a gas of inelastic particles, we find that the distribution function is close to a Gaussian for nearly elastic particles with coefficient of restitution close to 1. However, as the coefficient of restitution decreases, the distribution function becomes very different from a Gaussian, and is closer to an exponential distribution at the lowest coefficient of restitution e_n=0.6 considered here. The distribution function has a similar form for both smooth and rough particles. The variance of the distribution shows a significant decrease as the coefficient of restitution decreases, and it also decreases as the area fraction is increased.

In contrast to the relative velocity along the line joining the centers of the particles at contact, the relative velocity perpendicular to the line joining centers w_t, and the relative angular velocity ϖ, do not show a significant deviation from a Gaussian distribution, as shown in Fig. 21. The relative tangential velocity at contact is very well described by a Gaussian distribution, even when the distribution function is 1% of its maximum value at a high area fraction of 0.75. In addition, it is clear that the variance of the relative velocity

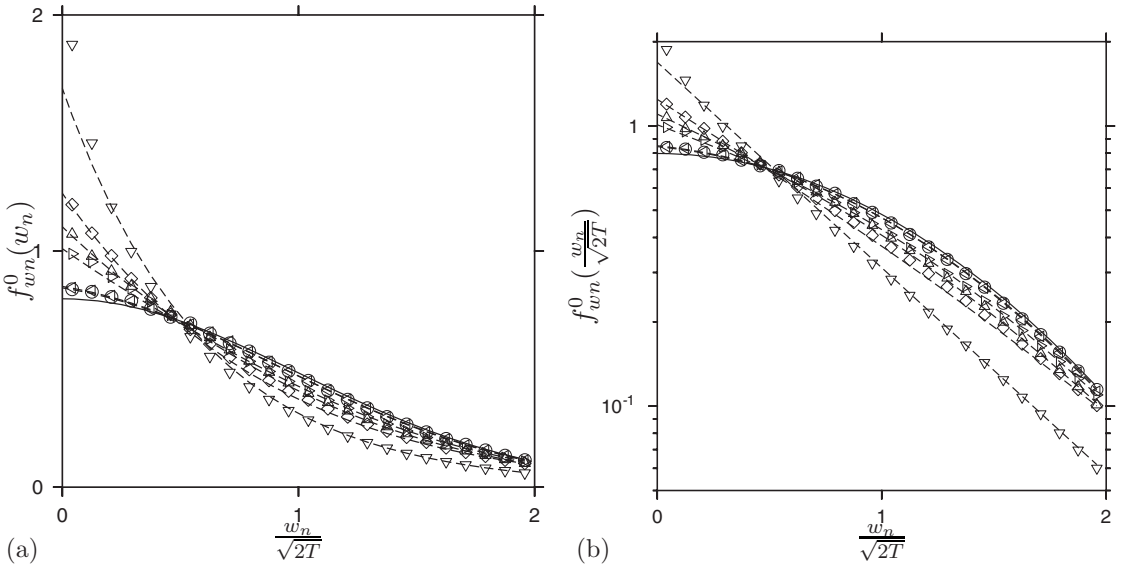

FIG. 19. The relative velocity distribution $f^{(0)}_{wn}(w_n)$ as a function of $w_n/\sqrt{2T}$ in (a) a linear plot and (b) semilogarithmic plot for area fraction ϕ=0.5 for rough particles with e_t=1.0 and e_n=0.95 (○), e_t=1.0 and e_n=0.8 (△), and e_t=1.0 and e_n=0.6 (▽), and for smooth particles with e_t=−1.0 and e_n=0.95 (◁), e_t=−1.0 and e_n=0.8 (▷), and e_t=−1.0 and e_n=0.6 (◇). The broken lines are the best fits of composite distribution function (37). The solid line shows the Gaussian distribution for elastic disks.

distribution along the tangential direction is two times the translational temperature, as expected for a gas of elastic particles at equilibrium.

Even though the relative velocity distribution along the line joining the centers is very different from a Gaussian, the single-particle velocity distributions are close to a Gaussian. Figure 22 shows that the single-particle velocity distributions along both the flow and gradient directions, as well as the angular velocity distribution, are well approximated by Gaussian distributions even at area fractions as high as 0.75 and coefficients of restitution as low as 0.6 for rough particles and 0.7 for smooth particles. This shows that, as in the case of the shear flow of three-dimensional spheres, the change in the form of the relative velocity distribution is not due to the change in the form of the single-particle velocity distribution, but rather due to the correlation in the velocities of neighboring particles.

The above analysis shows that while the single-particle velocity distribution and the relative velocity perpendicular to the line joining centers are well described by Gaussian

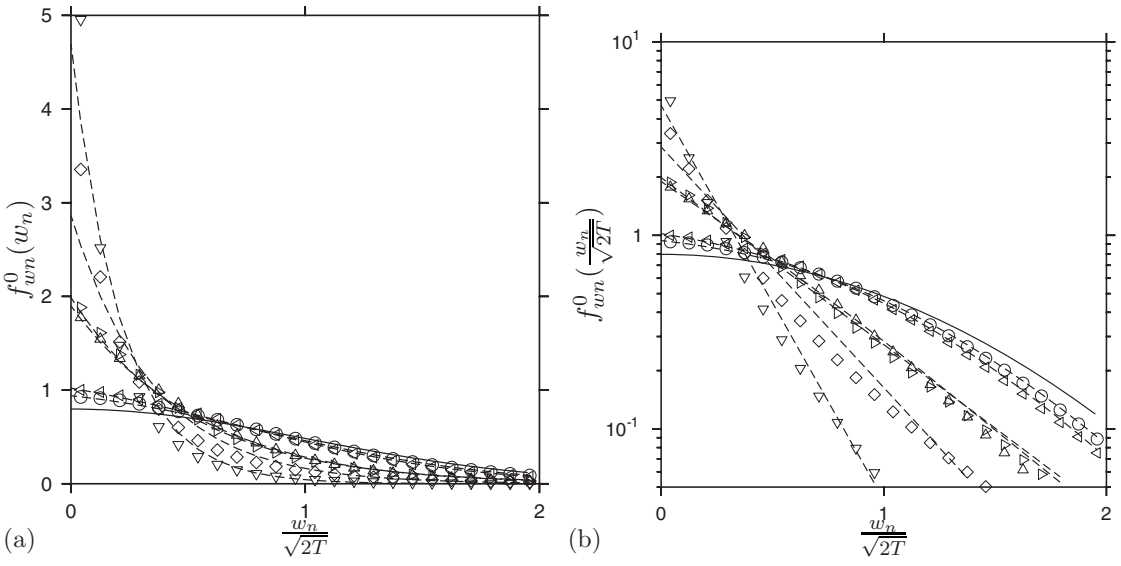

FIG. 20. The relative velocity distribution along the line joining the centers of the particles, $f^{(0)}_{wn}(w_n)$, as a function of $w_n/\sqrt{2T}$ in (a) a linear plot and (b) a semilogarithmic plot for area fraction ϕ=0.75 for rough particles with e_t=1.0 and e_n=0.95 (○), e_t=1.0 and e_n=0.8 (△), and e_t=1.0 and e_n=0.6 (▽), and for smooth particles with e_t=−1.0 and e_n=0.95 (◁), e_t=−1.0 and e_n=0.8 (▷), and e_t=−1.0 and e_n=0.7 (◇). The broken lines are the best fits of composite distribution function (37). The solid line shows the Gaussian distribution for elastic disks.

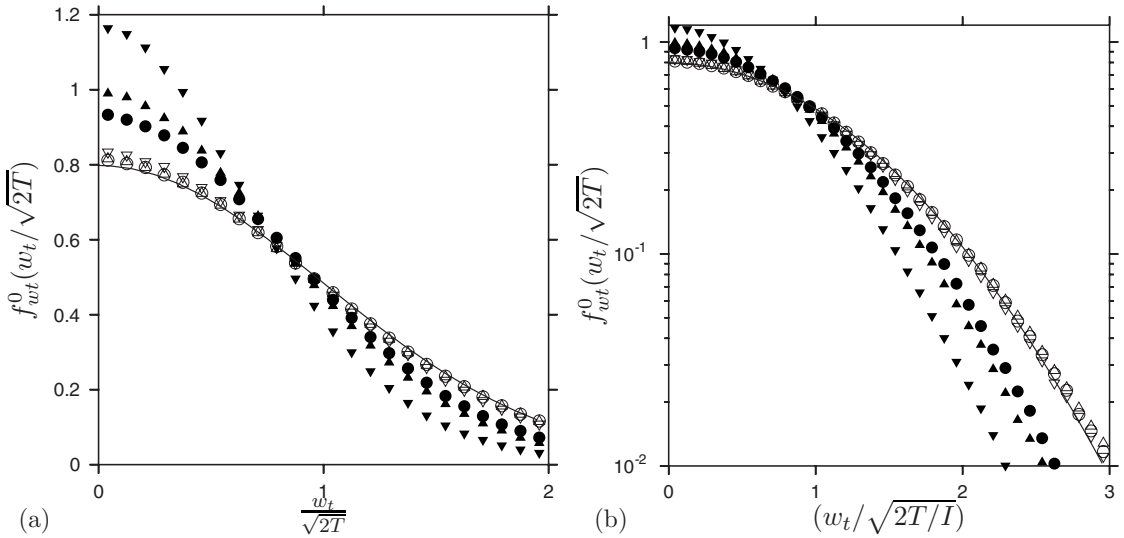

FIG. 21. The relative velocity distribution $f_{wt}^{(0)}(w_t/\sqrt{2T})$ as a function of $w_t/\sqrt{2T}$ (solid symbols) and the angular velocity distribution $f_{\varpi}^{(0)}(\varpi/\sqrt{2T/I})$ as a function of $\varpi/\sqrt{2T/I}$ (open symbols) in (a) a linear plot and (b) a semilogarithmic plot for area fraction $\phi=0.75$ for rough particles with $e_t=1.0$ and $e_n=0.95$ (○), $e_t=1.0$ and $e_n=0.80$ (△), and $e_t=1.0$ and $e_n=0.60$ (▽), and for smooth particles with $e_t=-1.0$ and $e_n=0.95$ (◁), $e_t=-1.0$ and $e_n=0.80$ (▷), and $e_t=-1.0$ and $e_n=0.70$ (◇). The solid line shows the Gaussian distribution for elastic disks.

distributions, the relative velocity along the line joining centers is very different from a Gaussian distribution. Therefore, it is necessary to have a good model for this distribution in order to calculate the stresses and the dissipation rate. For a three-dimensional sheared granular flow [22], it was found that the distribution function was well fitted by a composite distribution, consisting of the sum of a Gaussian and an exponential part, of the form

$$f_{wn}^{(0)}(w_n) = \frac{C}{1+e_n^{-1}}\alpha \exp(-\alpha w_n) + \frac{1-C}{\sqrt{\pi T_{wn}/2}(1+e_n^{-1})}\exp(-w_n^2/2T_{wn}), \quad (37)$$

where the parameter α is calculated from the distribution function obtained in the simulations using

$$\alpha = \left(\frac{6\int_0^\infty dw_n w_n^3 f_{wn}^{(0)}(w_n)}{\int_0^\infty dw_n w_n f_{wn}^{(0)}(w_n)} \right)^{-1/2} \quad (38)$$

and T_{wn}, the effective temperature for the relative normal velocity fluctuations, is given by

$$T_{wn} = \left(\frac{2\int_0^\infty dw_n w_n^3 f_{wn}^{(0)}(w_n)}{\int_0^\infty dw_n w_n f_{wn}^{(0)}(w_n)} \right) = \frac{3}{\alpha^2}. \quad (39)$$

The constant C in Eq. (37) is a fitted parameter, which is obtained by minimizing the mean square of the deviation of the actual distribution from composite distribution (37). We attempt to use fitted form (37) to fit the distribution in two dimensions as well. The composite distribution, shown by the broken lines in Figs. 19 and 20, are found to be in good agreement with the distribution function obtained from simulations for rough particles, even at the intermediate value of $e_n=0.8$, at which neither the Gaussian nor the exponential distribution provides a good fit.

The parameters α and C are shown as a function of e_n for different area fractions in Figs. 23 and 24. These graphs show many features which are identical to those observed for

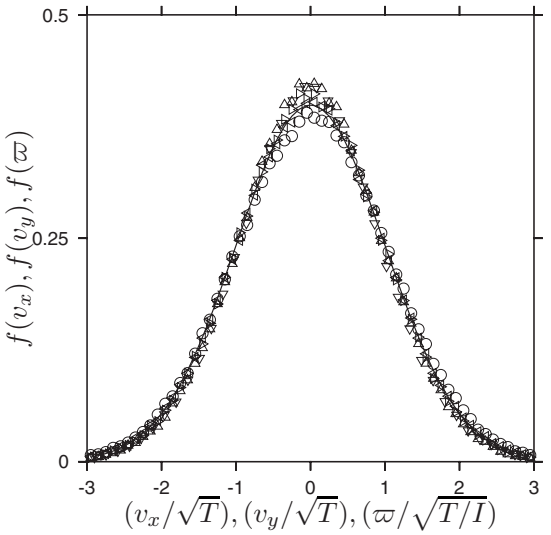

FIG. 22. The single-particle distribution functions for area fraction $\phi=0.75$. The different symbols are as follows: ○—$f(v_x)$ as a function of $v_x/\sqrt{T}$ for rough particles with $e_t=1$, $e_n=0.6$; △—$f(v_y)$ as a function of $v_y/\sqrt{T}$ for rough particles with $e_t=1$, $e_n=0.6$; ▽—$f(\varpi)$ as a function of $\varpi/\sqrt{T/I}$ for rough particles with $e_t=1$, $e_n=0.6$; ◁—$f(v_x)$ as a function of $v_x/\sqrt{T}$ for smooth particles with $e_t=-1$, $e_n=0.6$; and ▷—$f(v_y)$ as a function of $v_y/\sqrt{T}$ for smooth particles with $e_t=-1$, $e_n=0.6$. The solid line shows the Gaussian distribution for elastic disks in the absence of shear.

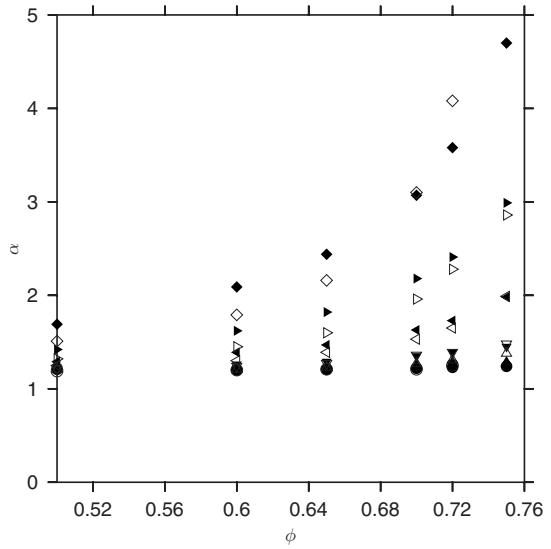

FIG. 23. The parameters α in normal velocity distribution (37) for e_n=0.98 (○), e_n=0.95 (△), e_n=0.9 (▽), e_n=0.8 (◁), e_n=0.7 (▷), and e_n=0.6 (◇), and for smooth particles e_t=−1.0 (open symbols) and e_t=1.0 (filled symbols).

a three-dimensional shear flow. It is observed that C is close to 1 for e_n=0.6,0.7. It decreases to about 0.5 for e_n=0.8, and is close to 0 for e_n=0.9 and 0.95. This indicates a clear change in the nature of the distribution function from a Gaussian to an exponential form at about e_n=0.8. However, unlike in the three-dimensional case, we find that the parameter C is not a constant, but seems to increase gradually as the area fraction is increased in two dimensions.

Next, we briefly analyze the components $g_{wn}^{(2)}$ and $h_{wn}^{(2)}$ defined in Eqs. (35) and (36). Rather than analyze the distributions themselves, we examine the ratios $g_{wn}^{(2)}/f_{wn}^{(0)}$ and $h_{wn}^{(2)}/f_{wn}^{(0)}$ in Fig. 25. The distribution ratio $h_{wn}^{(2)}/f_{wn}^{(0)}$ is nearly a constant for nearly elastic particles with e_n=0.95, but it does show some variation with the relative velocity as the coefficient of restitution is decreased. However, it should be noted from Fig. 20 that the distribution function $f_{wn}^{(0)}$ decreases by about 2 orders of magnitude when $w_n/\sqrt{2T}$ varies from 0 to 1, and the variation in $h_{wn}^{(2)}/f_{wn}^{(0)}$ is much smaller over this range. The ratio $g_{wn}^{(2)}/f_{wn}^{(0)}$ has an even smaller magnitude, though it does show a transition from negative to positive values at the lowest coefficient of restitution of 0.6. The variations in the components of the distribution are also very similar to those obtained for three-dimensional spheres [22], indicating that the nature of the variation in the relative velocity distribution is a system property which is independent of the dimensionality of the system.

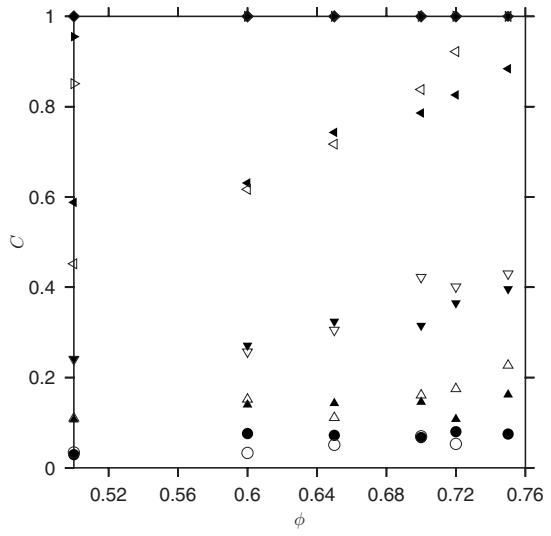

FIG. 24. The constant C in distribution function (37) as a function of area fraction at e_n=0.98 (○), e_n=0.95 (△), e_n=0.9 (▽), e_n=0.8 (◁), e_n=0.7 (▷), and e_n=0.6 (◇) and for smooth particles e_t=−1.0 (open symbols) and e_t=1.0 (filled symbols).

V. CONCLUSIONS

The system considered here was a two-dimensional shear flow of inelastic disks. The interaction between the disks is described by a collision model which contains two coefficients of restitution, the normal coefficient of restitution for the relative velocity along the line joining the centers and the tangential coefficient of restitution for the relative velocity perpendicular to the line joining the centers. Two types of particles are considered here, smooth particles, for which there is no change in the relative tangential velocity in a collision, and rough particles, where the relative tangential velocity is reversed in a collision. A homogeneous linear shear flow was generated using the Lees-Edwards boundary conditions. The event-driven simulation technique for hard disks was used, where the collisions are considered to be instantaneous. In the simulation, at a given instant, the collision times for pairs of particles are calculated on the basis of their positions and velocities, and the collision which occurs within the shortest time is determined. All particles are advanced by this time, and the velocities of the colliding particles are altered in accordance with the collision rules. Collision times are once again calculated and the procedure is repeated. The event-driven simulation technique suffers accumulation of computation errors at high area fractions when the time between collisions becomes numerically small, resulting in overlaps between particles, and so it cannot be implemented for area fractions very close to the close-packing area fraction. In two-dimensional disks, we also find that "shear banding" takes place at high area fractions, where two dense crystallized regions and nearly zero strain rate are separated by a relatively dilute shearing region. Since we are considering homogeneous shear flow, we have not been able obtain results after shear banding takes place. Shear banding is found to occur when the coefficient of restitution is greater than about 0.9, and the minimum area fraction for shear banding increases as the coefficient of restitution decreases. We do not find shear banding for coefficients of restitution less than 0.9, possibly due to the numerical errors resulting in particle overlaps at a lower area fraction.

Since there is no material time scale in the system (collisions are instantaneous), the only time scale is the inverse of the strain rate $\dot{\gamma}$ of the imposed flow. The granular temperature is proportional to $\dot{\gamma}^2$ through the energy balance equation. Therefore, the dynamics of the flow depends only on

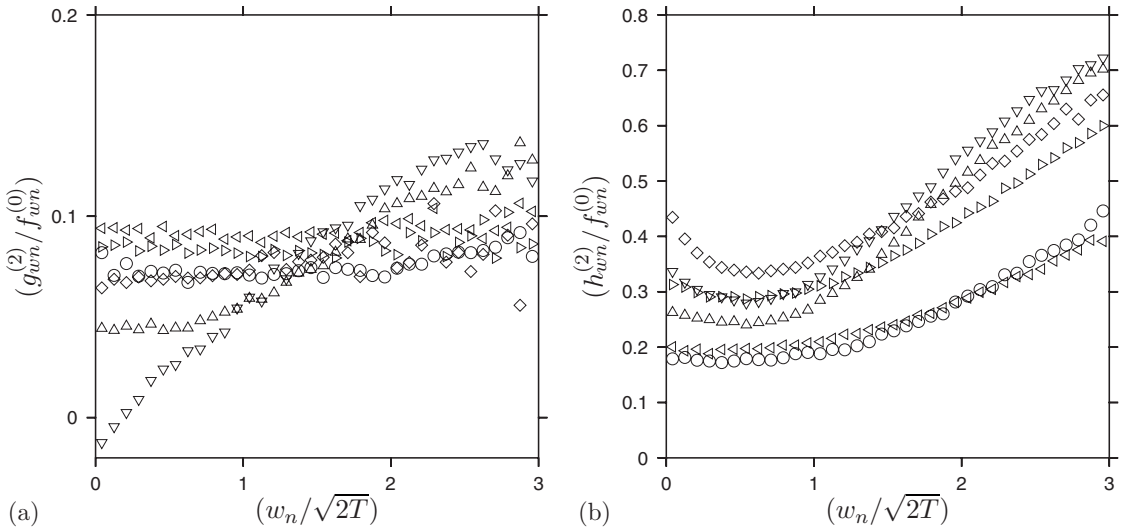

FIG. 25. The distribution ratios (a) $g^{(2)}_{wn}/f^{(0)}_{wn}$ and (b) $h^{(2)}_{wn}/f^{(0)}_{wn}$ as functions of $w_n/\sqrt{2T}$ for smooth particles with $e_t=-1.0$ and $e_n=0.95$ (○), $e_t=-1.0$ and $e_n=0.80$ (△), and $e_t=-1.0$ and $e_n=0.70$ (▽), and for rough particles with $e_t=1.0$ and $e_n=0.95$ (◁), $e_t=1.0$ and $e_n=0.80$ (▷), and $e_t=1.0$ and $e_n=0.70$ (◇).

the area fraction and the coefficients of restitution. By dimensional analysis, the collision frequency is proportional to $\dot{\gamma}$ times a function of the area fraction and coefficients of restitution, all components of the stress are proportional to $\dot{\gamma}^2$ times a function of the area fraction and coefficients of restitution, and the rate of dissipation of energy is proportional to $\dot{\gamma}^3$ times a function of the area fraction and the coefficients of restitution. The focus of our analysis has been to determine the dependencies of these dynamical quantities on the area fraction and the coefficients of restitution in the close-packing limit. Of particular interest is the comparison of the shear flow of two-dimensional disks with that of three-dimensional spheres studied earlier [21,22].

In the present analysis, we first examined the structure, or relative arrangement of particles, in a two-dimensional shear flow using the collisional order parameter q_6. It if found that shear does reduce the order parameter q_6, and increases the area fraction at which ordering takes place. However, partial ordering does take place even at the lowest area fractions considered here. This is in contrast to three-dimensional flows where there is a complete suppression of ordering by the mean shear. This difference could be due to the difference in the topological stabilities of two- and three-dimensional ordered structures. It is well known that a two-dimensional hexagonal close-packed structure is topologically stable to small changes in the position of the disks, whereas a three-dimensional face-centered-cubic structure is topologically unstable to small changes in the positions of the spheres [28,31]. In addition, it is well known that it is very difficult to obtain a glassy state of two-dimensional disks by rapid compression, since they tend to crystallize easily. In contrast, it is easier to realize glassy states for a three-dimensional hard-sphere system. All of these results are qualitatively in agreement with the present finding that shear has a smaller effect on the ordering of two-dimensional disks, in contrast to three-dimensional spheres. The difference in ordering also implies that the qualitative nature of the results for two-dimensional disks cannot be easily extrapolated to the shear flow of three-dimensional spheres. Figures 3 and 4 show, quite clearly, that the order parameter q_6 is independent of the coefficient of restitution for $e_n \leq 0.9$. There is some variation in the order parameter for nearly elastic particles with $e_n > 0.9$. But for $e_n \leq 0.9$, all the data collapse onto a universal curve which is very different from that for elastic particles. This indicates that if the particles are sufficiently inelastic, the state of order in the system does not depend on the specific value of the coefficient of restitution.

The variation in the collision frequency of the particles with the area fraction and coefficient of restitution was analyzed. For two-dimensional disks at equilibrium in the absence of shear, the collision frequency depends on the state of ordering of the system. For a crystallized state, the collision frequency diverges at the hexagonal-close-packing area fraction of about 0.91, but for the random-close-packed state, the divergence occurs at the random-close-packing area fraction of about 0.82. In the present analysis, for nearly elastic rough particles ($e_n=0.98$), we find that there is a gradual increase in the ordering as the area fraction is increased, in contrast to the nearly discontinuous increase in the order parameter for elastic disks in the absence of shear. Even though the collision frequency for $e_n=0.98$ is always higher than that for elastic particles in the absence of shear, the area fraction ϕ_{ad} at which the collision frequency diverges (by extrapolation of the data at high area fractions), referred to as the area fraction for arrested dynamics, is close to the hexagonal-close-packing area fraction of 0.91 for $e_n=0.98$. However, as the coefficient of restitution decreases, the value of ϕ_{ad} shows a decrease from about 0.85 at $e_n=0.8$ to a minimum of about 0.80 at $e_n=0.6$. The divergence of the collision frequency for smooth particles is more difficult to establish, due to the onset of shear banding when the collision frequency is still relatively small. However, the simulation results suggest that the qualitative behavior of the variation in the collision frequency with area fraction is similar for rough and smooth disks. For smooth particles, though

ϕ_{ad} decreases systematically as the coefficient of restitution is decreased, the dependence of the scaled collision frequency ν^* on $\phi_{ad}-\phi$ is independent of the coefficient of restitution, as indicated by Fig. 10(b). However, a similar data collapse is not evident for rough particles, and Fig. 10(a) clearly shows that there are small but perceptible difference in the dependence of ν^* on $\phi_{ad}-\phi$.

The divergence of the collision frequency has been discussed before in other contexts. It is implicitly present in theories which incorporate a pair distribution function which diverges at the random-close-packing volume fraction [33]. For a hard-particle system, since the collision frequency is proportional to $\sqrt{T}$ times the pair distribution function, the collision frequency also diverges. In kinetic theories for shear flows of granular materials [21,22], the temperature and the strain rate are coupled through the energy balance condition, and so the ratio of the collision frequency and the strain rate diverges when the pair distribution function diverges. The divergence is also present in theories of jamming [36], where the characteristic frequency, which reduces to the collision frequency in the unjammed state from energy balance arguments, diverges. The interesting issue here is that we find that the volume fraction for the divergence in the presence of shear depends on the coefficient of restitution of the particles, and it is not the same as that for a fluid of elastic particles at equilibrium. This has been incorporated in this section.

The qualitative behavior of the collision frequency obtained here is very different from that for three-dimensional spheres [21,22]. In the case of spheres, it was found that the close-packing volume fraction in the presence of shear is always smaller than the random-close-packing volume fraction (0.64) for elastic disks in the absence of shear. For the lowest coefficients of restitution $e_n=0.6$, the random-close-packing volume fraction was about 0.58, which is 10% lower than the value of 0.64 for elastic hard spheres in the absence of shear. In contrast, we find that for hard disks at the lowest coefficients of restitution $e_n=0.6$, the close-packing area fraction at which the frequency diverges, $\phi_{ad}=0.8$, is only about 2% lower than that for the random close packing of hard disks. At higher coefficients of restitution in the range of 0.8–0.9, ϕ_{ad} is in the range of 0.82–0.83, which is close to the random-close-packing area fraction for elastic hard disks. This is due to a combination of two effects, the decrease in the close-packing area fraction due to shear and the increase due to partial ordering. For this reason, it is also found that the pair distribution function previously derived by Luding [34] for two-dimensional disks in the absence of shear, which is designed to diverge at the random-close-packing area fraction of 0.82, is in good agreement with the simulation results for rough particles with coefficient of restitution in the range of 0.8–0.9, though it underestimates the collision frequency for coefficient of restitution of less than 0.8.

Even though the collision frequency diverges as the area fraction for arrested dynamics is approached, it is found that there is a much smaller variation in the granular temperature in this limit. There does appear to be an increase in the granular temperature for nearly elastic particles at $e_n=0.98$. But for lower coefficients of restitution, the granular temperature seems to approach a finite value. We find that the pressure is well predicted by the theory of Jenkins and Richman [2], provided the pair distribution function obtained from the simulations is used in the theoretical expression for the pressure. The pressure increases by about an order of magnitude when the area fraction increases from 0.3 to about 0.75. However, the ratio of the pressure to the collision frequency shows a relatively small variation, indicating that the collisional mechanism of stress transmission dominates at high area fractions. When scaled by the collision frequency, there is a variation of only a factor of about 3 over the same range. This clearly indicates that the collision frequency is the relevant variable in this case, rather than the temperature or the strain rate. Therefore, a much better data collapse is obtained by scaling the dynamical variables by the collision frequency rather than the pressure.

The first normal stress difference $[(\sigma_{xx}-\sigma_{yy})/p]$ was found to be numerically small for all the area fractions and coefficients of restitution studied here. The first normal stress difference was found to be positive at low area fractions, but became negative at the highest area fractions studied here. The magnitude of the first normal stress difference is less than 0.2 for the lowest area fraction of 0.5 and the lowest coefficient of restitution of $e_n=0.6$, and the magnitude decreased as the area fraction increased. This indicates that the approximation of an isotropic pressure is a good one for a dense flow of inelastic disks, and this assumption gets better as the area fraction approaches the close-packing area fraction.

The ratio of the shear stress to pressure was examined and compared with the theoretical results of Jenkins and Richman [2]. It was found that the numerical value of the ratio predicted by the theory is quite close to that obtained from simulations, and the difference is only about 50% at the highest area fraction and the lowest coefficient of restitution considered here. However, there is a large qualitative difference in the nature of the variation in σ_{xy}/p with area fraction. The constitutive relations from theory predict that σ_{xy}/p always increases with area fraction in the close-packing limit. In contrast, in the simulations, we find that the ratio σ_{xy}/p decreases as the area fraction increases for coefficient of restitution e_n less than about 0.9. This difference is significant because σ_{xy}/p can also be physically interpreted, for the flow down an inclined plane, as $\tan(\theta)$, where θ is the angle with respect to the horizontal. For a stable flow to exist, it is necessary for σ_{xy}/p to decrease as the area fraction increases near the close-packing limit. Since the constitutive relations of Jenkins and Richman [2] always predict the opposite, it has been assumed that kinetic theories are not applicable for the flow of granular materials down an inclined plane. The present simulations show though there is a relatively small difference in the numerical value of σ_{xy}/p between theory and simulations, this does result in a change in the slope of the σ_{xy}/p versus area fraction curve. The simulation results have the correct slope required for a stable flow for coefficients of restitution of less than about 0.9.

The rate of dissipation of energy is not well predicted by the theoretical expressions of Jenkins and Richman [2], however, even when the pair distribution function obtained from simulations is used. At the lowest coefficient of restitution of about 0.6, the theoretical prediction for the dissipation rate is

about 1 order of magnitude higher than that obtained from simulations. A similar feature was observed for the three-dimensional flow of inelastic spheres [21,22], and the reason for the difference was found to be the difference in the forms of the distribution of relative velocities between pairs of colliding particles. This motivated a detailed analysis of the distribution of relative velocities between colliding disks in the present study. In the case of smooth particles, we have examined the distribution of the relative velocity along the line joining the centers of the two disks. For rough particles, the relative velocity in the direction perpendicular to the line joining centers has also been analyzed. In all cases, we find that the single-particle velocity distributions in the flow and gradient directions, as well as the angular velocity distribution for rough particles, are very close to a Gaussian distribution, even when the relative velocity distribution is very different from a Gaussian distribution.

First, we discuss the relative velocity distribution along the direction of the line joining the centers of the disks. For elastic disks at equilibrium in the absence of shear, the relative velocity distribution is a Gaussian, with a variance equal to $2T$, where T is the temperature of the system. For nearly elastic particles ($e_n=0.98$), the relative velocity distribution is found to be a Gaussian, with a variance close to $2T$. However, as the coefficient of restitution decreases, the relative velocity distribution undergoes a transition to an exponential distribution, and the variance of the distribution is significantly smaller than $2T$. This qualitative behavior is identical to that for the shear flow of inelastic spheres in three dimensions, and indicates a significant correlation in the velocities of the colliding particles. For rough particles, in the direction perpendicular to the line joining centers, the velocity distribution function is close to a Gaussian even when the coefficient of restitution is as low as 0.6, and strong correlation effects are not observed.

This change in the form of the relative velocity distribution has a significant effect on the dynamical properties. This is because in the limit of high area fraction, the transmission of stress occurs mainly due to collisions, and the dissipation of energy is only due to collisions. The collision frequency, the stresses and the dissipation rate are proportional to the first, second, and third moments of the relative velocity distribution. In kinetic theories (Jenkins and Richman [2]), the Enskog approximation (the two-particle velocity distribution is the product of the single-particle velocity distributions) is assumed. This approximation results in a relative velocity distribution which is always Gaussian with a variance equal to $2T$ if the single-particle velocity distribution is a Gaussian. In the simulations, it is found that the relative velocity distribution is closer to an exponential at low coefficients of restitution, with a variance much smaller than $2T$. Since the variance is overestimated in the theory, the ratio of the pressure to the collision frequency (or pair distribution function) is overestimated, and the ratio of the dissipation rate to collision frequency is also overestimated. This explains the discrepancy between the dissipation rate from theory and simulations which has been the subject of much study.

There are two important conclusions that can be drawn with regard to the comparison of the dynamics of dense sheared granular flows in two and three dimensions. The structure and ordering in the shear flow of two-dimensional disks is very different form the shear flow of three-dimensional spheres. In the case of two-dimensional disks, there is partial ordering at high area fractions, even though the order parameter is lower than that in the absence of shear. The area fraction for arrested dynamics for sheared inelastic disks for coefficient of restitution e_n less than about 0.9 is close to the random-close-packing area fraction of 0.82 for elastic disks in the absence of shear. Due to this, the inelastic-hard-disk pair distribution function [34] is applicable, to a good approximation, for sheared inelastic hard disks as well. The second important conclusion is that the effect of correlations on the relative velocity distributions for sheared inelastic disks is found to be very similar to that for sheared inelastic spheres in three dimensions. It is found that the distribution changes in form from a Gaussian distribution for nearly elastic particles to an exponential distribution at the lowest coefficients of restitution studied here. A very similar form for the relative velocity distribution was also observed for sheared inelastic spheres in three dimensions [21,22]. This correlation results in the significant overestimation of the dissipation rate in kinetic theories where the Enskog approximation is used, resulting in a relative velocity distribution which is close to a Gaussian.

ACKNOWLEDGMENT

This research was supported by the Department of Science and Technology, Government of India.

[1] S. B. Savage and D. J. Jeffrey, J. Fluid Mech. **110**, 255 (1981).
[2] J. T. Jenkins and M. W. Richman, Arch. Ration. Mech. Anal. **87**, 355 (1985).
[3] C. K. K. Lun, S. B. Savage, D. J. Jeffrey, and N. Chepurniy, J. Fluid Mech. **140**, 223 (1984).
[4] V. Kumaran, Phys. Rev. E **57**, 5660 (1998).
[5] N. Sela, I. Goldhirsch, and S. H. Noskowicz, Phys. Fluids **8**, 2337 (1996).
[6] N. Sela and I. Goldhirsch, J. Fluid Mech. **361**, 41 (1998).
[7] V. Kumaran, J. Fluid Mech. **506**, 1 (2004).
[8] V. Kumaran, J. Fluid Mech. **561**, 1 (2006).
[9] N. Mitarai and H. Nakanishi, Phys. Rev. Lett. **94**, 128001 (2005).
[10] L. E. Silbert, G. S. Grest, R. Brewster, and A. J. Levine, Phys. Rev. Lett. **99**, 068002 (2007).
[11] K. A. Reddy and V. Kumaran, Phys. Rev. E **76**, 061305 (2007).
[12] L. E. Silbert, D. Ertas, G. S. Grest, T. C. Halsey, D. Levine, and S. J. Plimpton, Phys. Rev. E **64**, 051302 (2001).
[13] M. H. Ernst, B. Cichocki, J. F. Dorfman, J. Sharma, and H. van

Beijeren, J. Stat. Phys. **18**, 237 (1978).
[14] V. Kumaran, Phys. Rev. E **79**, 011301 (2009).
[15] V. Kumaran, Phys. Rev. E **79**, 011302 (2009).
[16] A. V. Orpe, V. Kumaran, K. A. Reddy, and A. Kudrolli, Europhys. Lett. **84**, 64003 (2008).
[17] D. Ertas and T. C. Halsey, Europhys. Lett. **60**, 931 (2002).
[18] G. Lois, A. Lemaitre, and J. M. Carlson, Phys. Rev. E **72**, 051303 (2005).
[19] J. T. Jenkins, Phys. Fluids **18**, 103307 (2006).
[20] J. T. Jenkins, Granular Matter **10**, 47 (2007).
[21] V. Kumaran, J. Fluid Mech. (to be published).
[22] V. Kumaran, J. Fluid Mech. (to be published).
[23] N. Mitarai and H. Nakanashi, Phys. Rev. E **75**, 031305 (2007).
[24] M. P. Allen and D. J. Tildesley, *Computer Simulation of Liquids* (Clarendon, Oxford, 1992).
[25] D. Goldman, M. D. Shattuck, C. Bizon, W. D. McCormick, J. B. Swift, and H. L. Swinney, Phys. Rev. E **57**, 4831 (1998).
[26] S. Luding and S. McNamara, Granular Matter **1**, 113 (1998).
[27] M. Alam and C. M. Hrenya, Phys. Rev. E **63**, 061308 (2001).
[28] V. S. Kumar and V. Kumaran, J. Chem. Phys. **123**, 074502 (2005).
[29] L. V. Woodcock, J. Chem. Soc., Faraday Trans. 2 **72**, 1667 (1976).
[30] B. D. Lubachevsky and F. H. Stillinger, J. Stat. Phys. **60**, 561 (1990).
[31] J. P. Troadec, A. Gervois, and L. Oger, Europhys. Lett. **42**, 167 (1998).
[32] S. Chapman and T. G. Cowling, *The Mathematical Theory of Non-uniform Gases* (Cambridge University Press, Cambridge, England, 1970).
[33] S. Torquato, Phys. Rev. E **51**, 3170 (1995).
[34] S. Luding, Phys. Rev. E **63**, 042201 (2001).
[35] V. Kumaran, J. Fluid Mech. **599**, 120 (2008).
[36] M. Otsuki and M. Hayakawa, Prog. Theor. Phys. **121**, 647 (2009).